



Tong, L. et al. (2020) Discovery of [11C]MK-6884: a positron emission tomography (PET) imaging agent for the study of M4 muscarinic receptor positive allosteric modulators (PAMs) in neurodegenerative diseases. *Journal of Medicinal Chemistry*, 63(5), pp. 2411-2425. (doi: [10.1021/acs.jmedchem.9b01406](https://doi.org/10.1021/acs.jmedchem.9b01406)).

This is the author's final accepted version.

There may be differences between this version and the published version. You are advised to consult the publisher's version if you wish to cite from it.

<http://eprints.gla.ac.uk/211315/>

Deposited on: 28 February 2020

Enlighten – Research publications by members of the University of Glasgow
<http://eprints.gla.ac.uk>

Discovery of [¹¹C]MK-6884: A Positron Emission Tomography (PET) Imaging Agent for the Study of M4 Muscarinic Receptor Positive Allosteric Modulators (PAMs) in Neurodegenerative Diseases

Ling Tong^a, * Wenping Li^b, Michael Man-Chu Lo^c, Xiaolei Gao^c, Jenny Miu-Chen Wai^a, Michael Rudd^a, David Tellers^a, Aniket Joshi^b, Zhizhen Zeng^b, Patricia Miller^b, Cristian Salinas^b, Kerry Riffel^b, Hyking Haley^b, Mona Purcell^b, Marie Holahan^b, Liza Gantert^b, Jeffrey W. Schubert^a, Kristen Jones^a, James Mulhearn^a, Melissa Egbertson^a, Zhaoyang Meng^a, Barbara Hanney^a, Robert Gomez^a, Scott T. Harrison^a, Paul McQuade^b, Tjerk Bueters^d, Jason Uslander^e, John Morrow^e, Fiona Thomson^e, Jongrock Kong^f, Jing Liao^f, Oleg Selyutin^c, Jianming Bao^c, Nicholas B. Hastings^e, Sony Agrawal^e, Brian C. Magliaro^e, Frederick J. Monsma, Jr.^e, Michelle D. Smith^e, Stefania Rizzo^e, David Hesk^f, Eric Hostetler^b, and Robert Mazzola^c

^aDiscovery Chemistry, Merck & Co., Inc., 770 Sumneytown Pike, West Point, PA 19486, USA

^bTranslational Biomarkers, Merck & Co., Inc., 770 Sumneytown Pike, West Point, PA 19486, USA

^cDiscovery Chemistry, Merck & Co., Inc., 2000 Galloping Hill Road, Kenilworth, NJ 07033, USA

^dPharmacokinetics, Pharmacodynamics and Drug Metabolism, Merck & Co., Inc., 770 Sumneytown Pike, West Point, PA 19486, USA

^eDiscovery Biology, Merck & Co., Inc., 770 Sumneytown Pike, West Point, PA 19486, USA

^fDepartment of Process Research and Development, Merck & Co., Inc., 126 E. Lincoln Ave. Rahway, NJ 07065, USA

**Ling.Tong@merck.com*

ABSTRACT: The measurement of receptor occupancy (RO) using positron emission tomography (PET) has been instrumental in guiding discovery and development of CNS directed therapeutics. We and others have investigated muscarinic acetylcholine receptor 4 (M4) positive allosteric modulators (PAMs) for the treatment of symptoms associated with neuropsychiatric disorders. In this article, we describe the synthesis, in vitro, and in vivo characterization of a series of central pyridine-related M4 PAMs that can be conveniently radiolabeled with carbon-11 as PET tracers for the in vivo imaging of an allosteric binding site of the M4 receptor. We first demonstrated its feasibility by mapping the receptor distribution in mouse brain and confirming that a lead molecule **1** binds selectively to the receptor only in the presence of the orthosteric agonist carbachol. Through a competitive binding affinity assay and a number of physiochemical properties filters, several related compounds were identified as candidates for in vivo evaluation. These candidates were then radiolabeled with ¹¹C and studied in vivo in rhesus monkeys. This research eventually led to the discovery of the clinical radiotracer candidate [¹¹C]MK-6884.

INTRODUCTION

There were an estimated 46.8 million people worldwide living with dementia in 2015 and this number is believed to have grown to 50 million people in 2017.¹ Alzheimer's disease (AD) is the major cause of dementia in the elderly.² While progressive cognitive decline is a hallmark

symptom of dementia, the condition is also strongly associated with psychiatric and behavioral symptoms such as hallucinations, delusions, persistent aggression, severe agitation, and risk of harming others. These behavioral symptoms are the main drivers for institutionalization.³ Currently, there is a significant unmet medical need for efficacious and safe drugs to alleviate behavioral disturbances in these patients.³

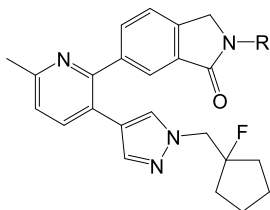
Muscarinic acetylcholine receptors (mAChR) are members of the G protein-coupled receptor superfamily that mediates the actions of the neurotransmitter acetylcholine in both the central and peripheral nervous system.⁴ Five distinct muscarinic receptors (M1-M5) have been identified in mammals. In the central nervous system (CNS), these receptors play a critical role in mediating higher cognitive processing and control of dopamine release.⁴ Clinical studies with xanomeline, an M1/M4 preferring agonist, have demonstrated that stimulating the muscarinic cholinergic system is a viable treatment for alleviating psychosis and behavioral disturbances in AD and schizophrenia patients.⁵⁻¹⁰ However, xanomeline, like other muscarinic agonists, failed in further clinical development due to an intolerable adverse side effect profile, presumably resulting from a lack of adequate receptor subtype selectivity.¹¹⁻¹⁴ The M4 muscarinic acetylcholine receptor is predominantly expressed in the striatum, as well as in the hippocampus and cortex.¹⁵ It has been implicated in several CNS disorders.¹⁶ Preclinical experiments identified the M4 receptor as the mAChR subtype responsible for antipsychotic-like efficacy as well as modest cognitive enhancement.¹⁷ M4 positive allosteric modulators are anticipated to provide a greater opportunity for target selectivity compared to an orthosteric agonist, as they bind to a site that is distinct from that of the endogenous ligand. This feature may translate to an improved clinical safety and tolerability profile.¹⁷⁻²⁵ Moreover, allosteric modulation may offer potential

advantages such as maintaining both spatial and temporal neurotransmission through modulation of physiologically relevant receptor-mediated neural signaling pathways.¹⁷⁻²⁵

Noninvasive imaging of M4 PAMs using positron emission tomography (PET) allows quantification of the distribution, expression, and modulation of this receptor under physiological and pathological conditions. With a validated PET ligand to the receptor, PET can be used to assess receptor occupancy (RO) of a drug candidate at the same receptor, thereby defining its pharmacodynamic profile and identifying therapeutically relevant dose ranges. In general, the PET tracer should provide high specific signal (total/non-specific $\geq 1.5:1$) to allow the quantitative mapping of the target of interest. It should have in vivo displaceable binding suitable to determine pharmacokinetics (PK)/RO relationships in preclinical species and humans. In vitro binding potential (BP_{ND}), defined as the ratio of available receptor sites (B_{max}) to the equilibrium distribution constant (K_d), should be > 10 in the highest receptor density region. In addition, the chemical structure of the tracer should be amenable to radionuclide incorporation (^{11}C , ^{18}F) using routes that can be reliably executed at clinical PET centers. To realize these goals, the tracer should have the following properties: high permeability ($P_{app} > 20 \times 10^{-6}$ cm/s), non-substrate of efflux transporters such as P-glycoprotein (P-gp) (transport ratio < 2), and low to moderate lipophilicity (shake-flask Log D < 3.5) to avoid high non-specific binding.^{26, 27}

We previously communicated the discovery of a lead series exemplified by compound **1** (Figure 1), a potent M4 PAM with adequate mAChR subtype selectivity over the other muscarinic receptors subtypes.²⁸ To support the concurrent discovery program aiming at the identification of a suitable M4 PAM for clinical development, we started a research program to develop a PET tracer for in vivo imaging of the M4 allosteric binding site in brain. In this

article, we describe the work leading to the identification of an M4 PAM PET tracer, [^{11}C]MK-6884 (**13**).²⁹



1 R = CH₃; [^3H]**1** R = CT₃; [^{11}C]**1** R = $^{11}\text{CH}_3$

Human FLIPR IP = 16 nM

K_d = 17.6 nM

sFLog D = 2.5

P-gp (h/r) = 1.2/7.2

P_{app} = 29.5 x 10⁻⁶ cm/s

Figure 1. Compound **1**,²⁸ [^3H]**1**, [^{11}C]**1**

RESULTS AND DISCUSSION

The tritium-labeled analog of **1** (Figure 1) provided us with a good starting point to study the feasibility of developing an allosteric M4 PET tracer and to explore the relationship between receptor binding and function, as it is an M4 PAM ligand with high affinity ($K_i = 3.1$ nM) and good physicochemical properties (sF logD = 2.5). Our discovery efforts began with mapping M4 receptor distribution, concentration (B_{max}), binding specificity, and selectivity. First, autoradiography was performed using 5 nM of [^3H]**1** in brain tissue from wild type (WT) and M4 knock out (KO) mice in the presence of 10 μM carbachol, a stable orthosteric mAChR agonist (Figure 2). The highest binding density was found in mouse brain striatum (135 optical density or O.D. units), moderate binding in cortex (36 O.D. units) and thalamus (25 O.D. units),

and negligible displaceable binding in cerebellum (< 10 O.D. units). Minimal binding in all regions was observed in the absence of carbachol. Minimal binding was also observed in the presence of carbachol in brain tissue from M4 KO mice. The results demonstrated that binding of [^3H]**1** is dependent on the presence of an orthosteric agonist and M4 specific (Figure 2).

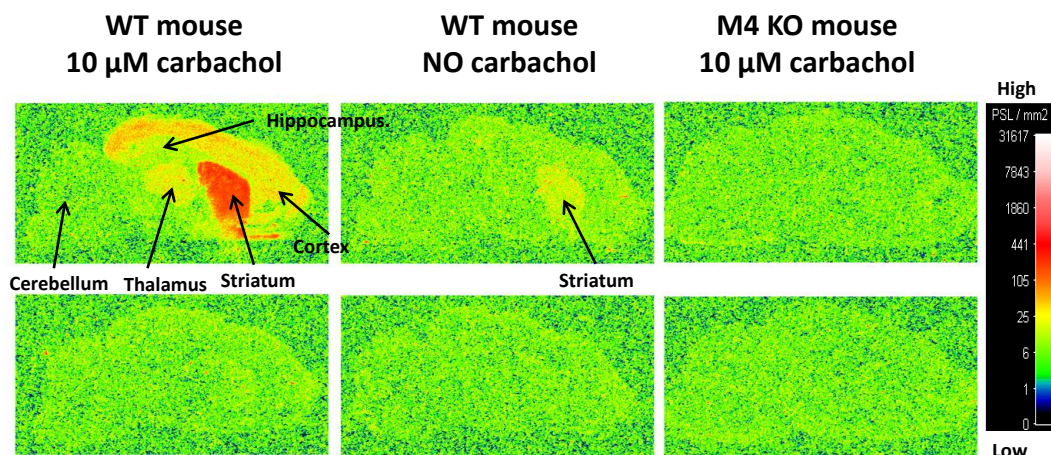


Figure 2. Upper panels: total binding of [^3H]**1** in mouse brain slices by in vitro autoradiography. Lower panels: non-displaceable binding was defined with unlabeled **1** (2 μM).

In rhesus monkey and human brain tissue homogenates, saturation binding studies show that [^3H]**1** binds to a single, saturable site, as determined by a non-linear curve fit (Figure 3). The K_d and B_{\max} values of [^3H]**1** in monkey and human striatum tissue are shown in Table 1. The density of M4 receptors is low (< 10 nM) in monkey and human, and while the K_d value for [^3H]**1** is moderate, the affinity is not sufficient to achieve a B_{\max}/K_d ratio greater than 10. Subsequently, compound **1** was radiolabeled with [^{11}C]methyl iodide and studied in vivo in rhesus monkey to evaluate brain uptake and specific binding to the M4 PAM binding site. As expected, based on the binding affinity (K_d), [^{11}C]**1** did not show specific signal, despite having appropriate lipophilicity and permeability properties.

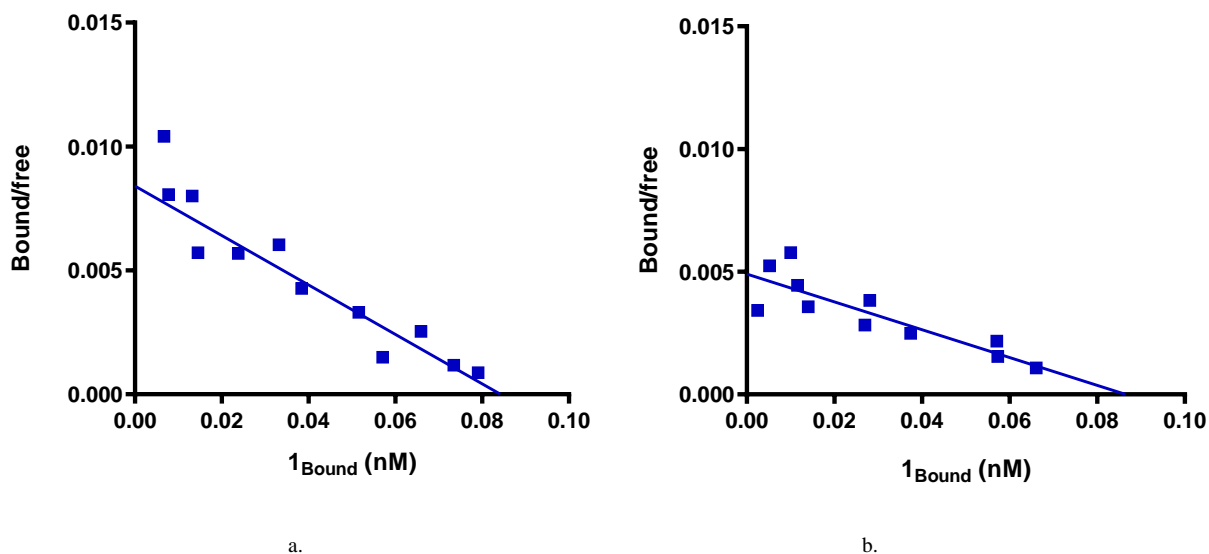


Figure 3. Scatchard analysis of saturation binding studies with [³H]**1** in a) rhesus monkey striatum homogenates; b) human striatum homogenates.

Table 1. B_{max} and K_d values for [³H]**1** in rhesus monkey and human striatum measured in the presence of 10 μM carbachol

	K _d (nM)	B _{max} (nM)
Rhesus monkey striatum ^a	12.8	7.7
Human striatum ^b	17.6	7.2

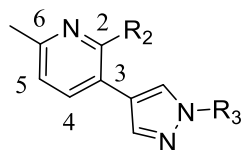
a) average of two determinations; b) single determination

We hypothesized that further improvement in binding affinity was necessary, while maintaining optimal physicochemical properties. We started by identifying analogs that are amenable to radiolabeling and potent against M4 PAM, as measured by FLIPR. We then selected these analogs for measurement of M4 binding affinity (K_i), which was determined using competition binding of M4 allosteric analogs (in the presence of 10 μM ACh) at human M4 receptors expressed in Chinese hamster ovary (CHO) cells with [³H]**1**. Table 2 lists compounds

with fixed R₆ methyl substitution on the central pyridine ring. Using compound **1** as a starting point, we first altered the tail group R₃ off the nitrogen of pyrazole while keeping the R₂ lactam group constant. Methyl substitution on the tertiary position of the cyclopentyl group improved binding affinity (compound **2**; K_i = 1.0 nM) compared to the fluoro-substituted compound **1** (K_i = 3.1 nM). An open carbo-chain tail was detrimental to the binding affinity (compound **3**; K_i = 9.8 nM). Distal fluoro-substitution on the cyclopentyl group also decreased the binding affinity (compound **4**; K_i = 15 nM) when compared to the unsubstituted cyclopentyl compound **5** (K_i = 2.9 nM). A bridged *[1.1.1]* bicyclic group also decreased the binding affinity slightly to 5.2 nM (compound **6**), while a cyclohexyl group with bis-fluoro-substitution at the 4-position further reduced the binding affinity with a K_i of 14 nM (compound **7**). A cyclopropyl ring as the tail group is also unsuitable for improving the affinity (compound **8**) as K_i dramatically increases to 30 nM. From this exercise, we concluded that a 5-membered ring system was optimal for M4 binding affinity.

Next, we screened a small number of R₂ substitutions on the pyridine ring that would allow for radiolabeling. Methoxycinnoline as R₂ combined with (methylcyclopentyl)methyl group as R₃ improved the binding affinity into the sub-nanomolar range (compound **9**, K_i = 0.6 nM). However, substituting the methoxy group in the cinnoline with the dimethylamino group failed to improve binding affinity (compound **10**, K_i = 4.9 nM). Another functional group, 2-methyl indazole, also showed detrimental effect on binding K_i as demonstrated by compound **11** with a K_i = 13 nM.

Table 2. FLIPR assay results and K_i of M4 PAMs: R₂ and R₃ variations

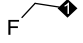
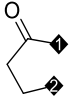


Compound	R ₂	R ₃	hM4 FLIPR IP (nM) ^{a,b,d}	K _i (nM) ^{c,d}
1			16 (12, 20)	3.1 (2.6, 3.7)
2			6.6 (5.3, 8.3)	1.0 (0.96, 1.0)
3			33 (28, 38)	9.8 (8.3, 12)
4 ^e			30 (21, 43)	15
5			17 (14, 20)	2.9 (2.0, 4.0)
6			18 (14, 22)	5.2
7			27 (23, 31)	14 (5.0, 37)
8			110 (71, 160)	30 (27, 34)
9			8.5 (7.0, 10)	0.6

10			40 (37, 43)	4.9 (4.0, 6.1)
11			57 (56, 58)	13 (12, 13)

a) Calcium mobilization FLIPR assays, IP values represent the geometric average of at least two experiments. b) The maximal efficacy normalized to the maximal efficacy of human ACh ranged from 90 to 109% for compounds **1** – **10**, and 80% for compound **11**. c) Competition binding K_i using [^3H]**1**, values represent the geometric average of at least two experiments. d) $n = 1$, single number in italics; $n = 2$, geometric mean reported, the italicized values in parentheses represent the two measurements; $n > 2$, geometric mean reported, the values in parentheses represent the lower and upper limits of the 95% confidence intervals. e) racemic isomers with trans stereochemistry.

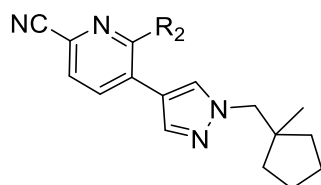
Next, we investigated R_4 , R_5 and R_6 substitutions on the central pyridine ring by fixing the R_2 group as the methyl lactam and the tail group on pyrazole (R_3) as the (methylcyclopentyl)methyl. The data are summarized in Table 3. When all three positions were unsubstituted, the binding affinity decreased to a K_i of 10 nM (compound **12**). Cyano-substitution at the 4- and 6-positions were examined, with 6-substituted cyano showing significant improvement in K_i (**13**, $K_i = 0.2$ nM) and 4-substituted cyano compound **16** displaying decreased binding affinity ($K_i = 22$ nM). Therefore, 6-cyano substitution was preferred over methyl for binding affinity (compound **13** vs. compound **2**). The preference of substitution on 5- and 6- positions was examined by fluorine atom in compound **14** and compound **15**, with substitution at the 6-position preferred (compound **14**, $K_i = 1.5$ nM; compound **15**, $K_i = 7.5$ nM). Bis-substitutions were also investigated in compounds **17–19**, which demonstrated similar K_i 's as compound **2**. A methyl fluoro group at the 6-position combined with 5-fluoro in compound **19** provided an alternative labeling handle (^{18}F). However, this combination did not show any advantage in terms of binding affinity. When the 5-position and 6-position were fused to make a cyclopentanone ring, the binding affinity improved significantly, as evident from compound **20** with a K_i of 0.2 nM.

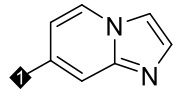
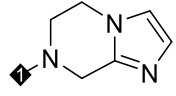
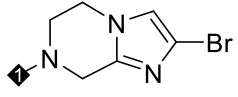
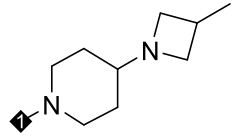
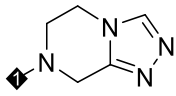
18	Me	Me	H	9.7 (9.1, 10)	1.0 (0.76, 1.4)
19		F	H	47 (43, 52)	1.7 (0.7, 4.1)
20			H	29 (28, 30)	0.16 (0.12, 0.21)

a) Calcium mobilization FLIPR assays, IP values represent the numerical average of at least two experiments. b) The maximal efficacy normalized to the maximal efficacy of human ACh ranged from 83 to 101% except for 74% for compound **15** and 52% for compound **20**. c) Competition binding K_i using [^3H]**1**, values represent the numerical average of at least two experiments. d) $n = 1$, single number in italics; $n = 2$, geometric mean reported, the italicized values in parentheses represent the two measurements; $n > 2$, geometric mean reported, the values in parentheses represent the lower and upper limits of the 95% confidence intervals.

Compound **13** exhibited promising affinity, and the R_6 cyano substituent could be used to incorporate an ^{13}C label. This approach provided an opportunity to investigate a wider variety of R_2 groups. Several additional bicyclic ring systems were examined and summarized in Table 4. Imidazopyridine exhibited reduced binding affinity compared to the lactam (compound **21**, $K_i = 3.8$ nM vs. compound **13**, $K_i = 0.2$ nM). Promisingly, R_2 azacycles displayed subnano molar binding affinity (compounds **22–25**). The R_2 azacycles in compounds **22**, **23** and **25** were 6,5-fused bicyclic systems and a 4-(azetidin-1-yl)piperidine in compound **24**.

Table 4. FLIPR assay results and K_i of M4 PAMs: variation of R_2 with fixed R_3 and R_6



Compound	R ₂	hM4 FLIPR IP (nM) ^{a,b,d}	K _i (nM) ^{c,d}
21		25 (20, 32)	0.65 (0.57, 0.75)
22		4.6 (3.0, 7.0)	0.20 (0.15, 0.25)
23		6.7 (6.4, 7.1)	0.12 (0.06, 0.21)
24		14 (13, 15)	0.24 (0.08, 0.71)
25		6.4 (3.7, 11)	0.62 (0.33, 1.2)

a). Calcium mobilization FLIPR assays, IP values represent the numerical average of at least two experiments. b). The maximal efficacy normalized to the maximal efficacy of human ACh ranged from 80 to 102%. c). Competition binding K_i using [³H]**1**, values represent the numerical average of at least two experiments. d). n = 1, single number in italics; n = 2, geometric mean reported, the italicized values in parentheses represent the two measurements; n > 2, geometric mean reported, the values in parentheses represent the lower and upper limits of the 95% confidence intervals.

With multiple compounds demonstrating significantly improved binding affinity (Tables 2-4) over compound **1**, the next step was to examine the physiochemical properties of these analogs and assess their likelihood of improved in vivo profiles. Analogs with sub-nanomolar binding affinity were selected (compounds **9**, **13**, **20**, **22**, **23**, **24** and **25**). In addition, we also selected compound **2** as an example with moderately improved K_i compared with compound **1**, which served as the baseline comparison. Table 5 summarizes the in vitro profiles of these analogs, including their K_i, P-gp efflux ratio, and apparent permeability (P_{app}). We have also included free fractions in plasma and in brain, as these parameters have been identified as useful

9		0.6	3.6	ND	ND	ND	ND	ND
13		0.19	2.9	2.7	0.7	28.8	17	4.3
20		0.16	2.4	ND	9.4	25	ND	ND
22		0.20	3.0	2.7	0.6	29	5.1	3.3
23		0.12	3.8	ND	0.8	23	ND	ND
24		0.24	3.3	ND	34	19	ND	ND
25		0.62	2.4	ND	8.4	26	ND	ND

a) K_i values from Tables 2–4. b) P-gp efflux ratio measured at 1 μ M in LLC-PK1 cell line expressing human (human LLC-MDR1) P-gp. A ratio of >2.5 indicates substrate liability. c) single determination. ND: not determined.

Compounds **2**, **13** and **22** showed overall acceptable physicochemical properties to merit further study. Compounds **2** and **13** were radiolabeled with [^{11}C]iodomethane ([^{11}C]CH $_3$ I) in the last step of the synthesis, while **22** was labeled with [^{11}C]HCN. Baseline PET scans for [^{11}C]**2**,

[¹¹C]**13** and [¹¹C]**22** in rhesus monkeys revealed non-displaceable binding potential (BP_{ND}) in striatum (Table 6). Although tracer [¹¹C]**2** did provide a measurable BP_{ND} (0.29), it was deemed too low for accurate quantification of the receptor occupancy of a therapeutic drug (Figure 4). The overall improved in vitro profile of compound **13** translated into an improved BP_{ND} of 0.83 in vivo. In contrast, despite sub-nanomolar binding affinity for compound **22**, it failed to further improve BP_{ND} in vivo (for compound [¹¹C]**22**, BP_{ND} = 0.2); time-activity curves and baseline PET images were very similar to [¹¹C]**2**. As previously described, non-specific tissue binding is important for the utility of a potential PET tracer in vivo. Compound **13** and **22** showed similar lipophilicity when measured by water–octanol partitioning, but behaved differently in biological matrices. The free fraction in rhesus plasma of compound **22** was approximately 3-fold lower compared to compound **13**. The free fraction in homogenized rat brain tissue also trended lower for compound **22**, suggesting higher non-specific binding in vivo (Table 5).

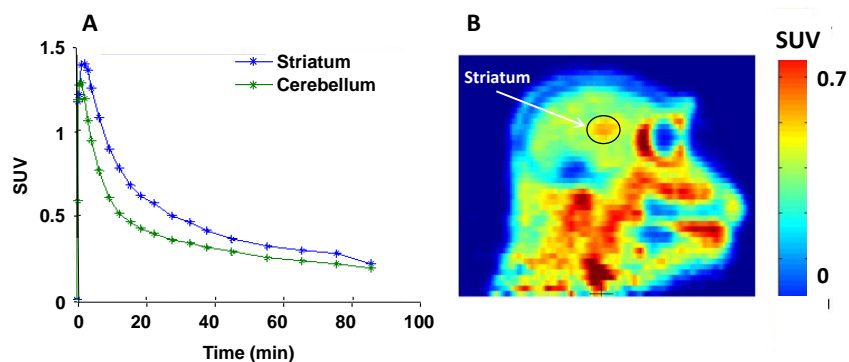
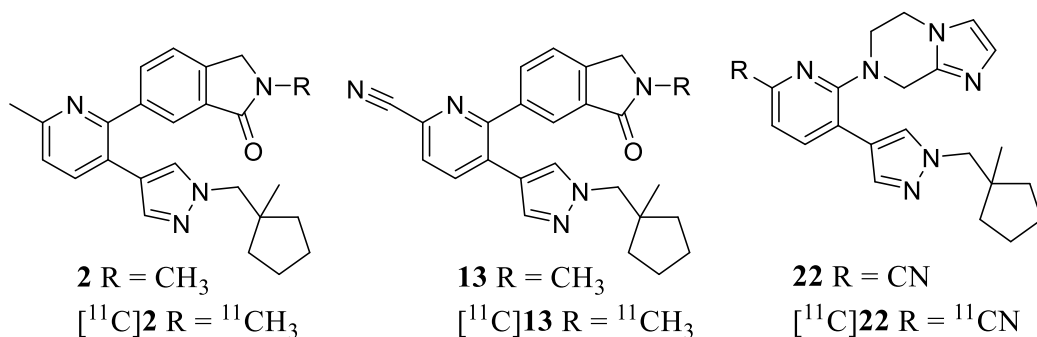


Figure 4. A: Time-activity curves in rhesus monkey striatum (blue) and cerebellum (green) for [¹¹C]**2** at baseline conductions. B: [¹¹C]**2** baseline PET image (0–90 minutes). Highest tracer uptake (red color) is in the striatum with very low tracer retention in all other regions.

Table 6. Measured in vivo BP_{ND} in rhesus monkey striatum for tracers [¹¹C]**2**, [¹¹C]**13** and [¹¹C]**22**

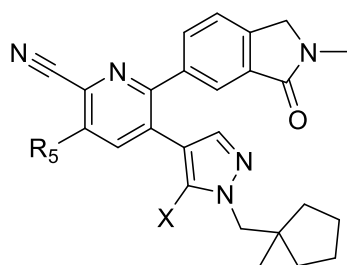


Compound	Striatum BP _{ND}
[¹¹ C] 2	0.29 ± 0.06 (4 scans in two monkeys)
[¹¹ C] 13	0.83 ± 0.17 (10 scans in five monkeys)
[¹¹ C] 22	0.1/0.2 (2 scans in one monkey)

With encouraging in vivo data obtained for compound **13**, we sought to further refine the structure of **13** to improve the binding potential BP_{ND}. We made additional modifications on R₅ and substitution X on the pyrazole. The data are summarized in Table 7. The binding affinity for compound **26** was similar to compound **13** (R₅ = Me, K_i = 0.26 nM). The lipophilicity for this compound measured by sFlogD was within the desirable range (3.1). It is also highly permeable and has no P-gp liabilities. However, when radiolabeled with [¹¹C]CH₃I and evaluated in a PET imaging study, [¹¹C]**26** failed to improve binding potential over [¹¹C]**13** (BP_{ND} = 0.37 for compound **26**, Table 7). Chloro-substitution at R₅ in compound **27** showed similar binding affinity as compound **26**. However, the addition of the chlorine atom increased HPLC Log D to 3.6, indicating potential for higher non-specific binding. Substitution on the pyrazole ring (labeled as X) was also studied. A fluorine at this position improved binding affinity when compared with the unsubstituted compound **13** (compound **28**, K_i = 0.08 nM,

Table 7). The physiochemical properties of compound **28** also met all the criteria for a potential PET tracer. However, larger halides or pseudohalides at X showed detrimental effect on binding affinity, as K_i for both compounds **29** and **30** were > 1 nM. From this group of compounds, compound **28** was radiolabeled with $[^{11}\text{C}]\text{CH}_3\text{I}$, and the BP_{ND} in monkey was determined to be 0.42 (Table 7), still lower than compound **13**. This result could be attributed to the higher non-specific binding of compound **28** observed during tracer studies, in line with the higher sF Log D value and higher brain tissue binding (Table 7).

Table 7. Further optimization of compound 13 scaffold.



13 $R_5 = X = \text{H}$

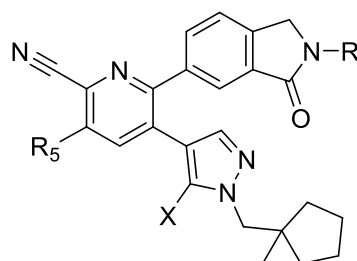
26 $R_5 = \text{CH}_3$; $X = \text{H}$

27 $R_5 = \text{Cl}$; $X = \text{H}$

28 $R_5 = \text{H}$; $X = \text{F}$

29 $R_5 = \text{H}$; $X = \text{Cl}$

30 $R_5 = \text{H}$; $X = \text{CN}$



$[^{11}\text{C}]\mathbf{13}$ $R_5 = \text{H}$; $X = \text{H}$; $R = [^{11}\text{C}]\text{CH}_3$

$[^{11}\text{C}]\mathbf{26}$ $R_5 = \text{CH}_3$; $X = \text{H}$; $R = [^{11}\text{C}]\text{CH}_3$

$[^{11}\text{C}]\mathbf{28}$ $R_5 = \text{H}$; $X = \text{F}$; $R = [^{11}\text{C}]\text{CH}_3$

Compound	K_i (nM) ^{a,b}	HPLC Log D ^d	sF Log D ^d	P_{gp} h ^c , d	P_{app} d	Fu% plasma (monkey) ^d	Fu% brain (rat) ^d	BP_{ND} of ^{11}C tracer
13	0.19	2.9	2.7	0.7	28.8	17	4.3	0.83
26	0.26 (0.20, 0.34)	3.2	3.1	1.0	25	11.4	3.2	0.37 ^d
27	0.13 (0.08, 0.20)	3.6	ND	0.7	27	2.9	ND	ND
28	0.08 (0.04, 0.19)	3.4	3.2	0.7	27	8.4	2.7	0.42 ^d
29	1.7 (1.0, 3.0)	3.7	ND	ND	ND	ND	ND	ND
30	2.0 (0.7, 5.5)	3.4	ND	ND	ND	ND	ND	ND

a) Competition binding K_i using [^3H]**1**, values represent the geometric average of at least two experiments. b) $n = 1$, single number in italics; $n = 2$, geometric mean reported, the italicized values in parentheses represent the two measurements; $n > 2$, geometric mean reported, the values in parentheses represent the lower and upper limits of the 95% confidence intervals. c) P-gp efflux measured at 1 μM in LLC-PK1 cell line expressing human (human LLC-MDR1) P-gp. A ratio of >2.5 indicates substrate liability; ND: not determined. d) single determination.

Since no further improvement of in vivo binding potential was achieved, efforts were focused on the in-depth characterization of **13** as a potential M4 PAM PET tracer clinical candidate. The molecular pharmacology profile of **13** as an M4 PAM was studied. Compound **13** was shown to be a PAM of ACh function in a cell-based Ca^{++} mobilization assay. In this assay, increasing concentrations of **13** potentiated the ability of a fixed concentration of ACh (EC_{20}) to mobilize intracellular Ca^{++} , with compound **13** exhibiting an EC_{50} of 27 nM. Further characterization of the allosteric nature of compound **13** was carried out by conducting a matrix of dose-response curves of ACh at 15 concentrations of **13**. A global curve fitting method was used to analyze the resulting curves according to a modified ternary complex model.^{31, 32} The shift parameters for compound **13** are summarized in Table 8, and shift curves are shown in Figure 5.

Table 8. FLIPR shift parameters for compound 13^a

species	α	Kb	$\tau\beta$
human	43 (32–78)	14 (6–22)	1.5 (1.2–1.6)
rhesus monkey	34 (32–36)	0.64 (0.55–0.74)	0.79 (0.71–0.88)

a) Binding Affinity (Kb), Cooperativity (α), and Intrinsic Efficacy ($\tau\beta$) estimates of test compounds on mAChR in the calcium mobilization assay in the presence of ACh for the human rhesus monkey receptors. b) All parameters reported as geometric means with the range of individual runs reported in parentheses. Human, $n = 3$; Rhesus monkey, $n = 2$.

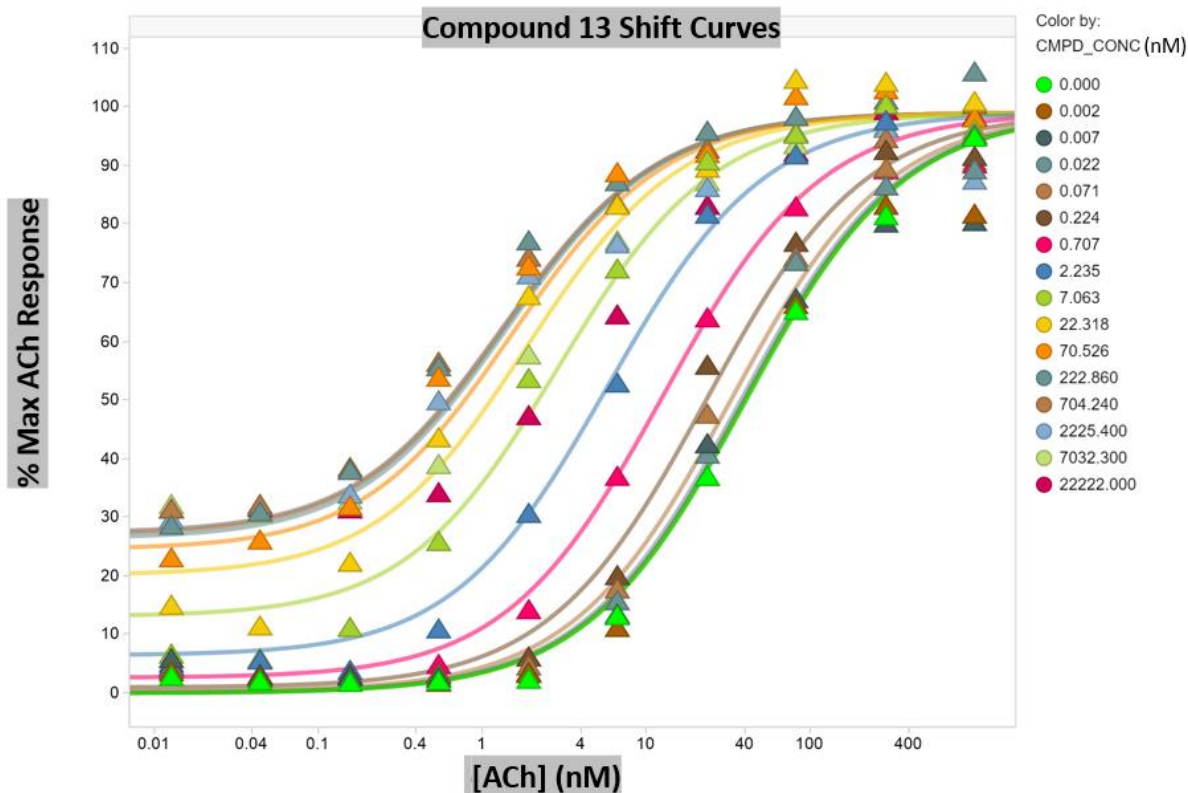
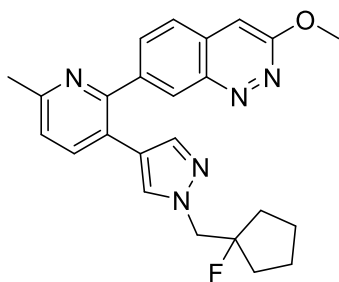


Figure 5. Compound **13** potentiation of ACh induced Ca^{++} mobilization in CHO-hM4-Gqi5 cells. Increasing concentrations of ACh were assayed for increases in Ca^{++} mobilization in the presence of 0-22 μM compound **13**, resulting in a leftward shift of the ACh dose response curve.

$[^{11}\text{C}]\mathbf{13}$ was further evaluated in five rhesus monkeys to assess brain uptake and specific binding to the M4 allosteric site. Baseline PET scans in five monkeys after a single intravenous administration revealed that $[^{11}\text{C}]\mathbf{13}$ rapidly penetrated the blood/brain barrier and distributed as expected based on the known presence of M4 receptors in the brain. The highest tracer uptake was noted in the striatum region, consistent with autoradiography results of $[^3\text{H}]\mathbf{1}$. A blockade experiment (Figure 7) was also carried out with compound **31** (Figure 6),²⁸ a potent M4 PAM. Injection of $[^{11}\text{C}]\mathbf{13}$ (189 MBq, 1.4 μg mass of **13**), following intravenous administration of 3 mg/kg compound **31**, resulted in significant reduction (receptor occupancy = 87%) in tracer

uptake in the striatum relative to the baseline PET scan with [¹¹C]**13**. This result indicated the ability of [¹¹C]**13** to determine an M4 PAM plasma/receptor occupancy relationship with a robust specific signal for structurally similar M4 PAM molecules.

An off-target screening of compound **13** was performed against a neuro panel of 115 receptors and enzymes by Eurofins Panlabs (Taipei, Taiwan). Compound **13** showed >3,600-fold selectivity against the majority of those targets, including other mAChRs in these binding assays. Compound **13** displayed only weak binding ($IC_{50} > 1\mu M$) to adenosine transporter. As PET tracers should have high affinity to show robust specific binding signal and are only administered as microdoses, off-target binding at the measured weak potencies is not expected to be a concern for the safety or imaging characteristics of [¹¹C]**13**. Additional off-target profiling of **13** in a high throughput ion channel flux assays revealed $IC_{50} > 30\mu M$ against Nav 1.5, Cav 1.2 and Ikr ion channels.



31

Human M4 FLIPR IP = 17 nM

Rat M4 FLIPR IP = 29 nM

M1/M4 IP ratio = 134

M2/M4 IP ratio >1700

M3/M4 IP ratio > 1700

M5/M4 IP ratio > 1700

Figure 6. Profile of compound **31**.²⁸

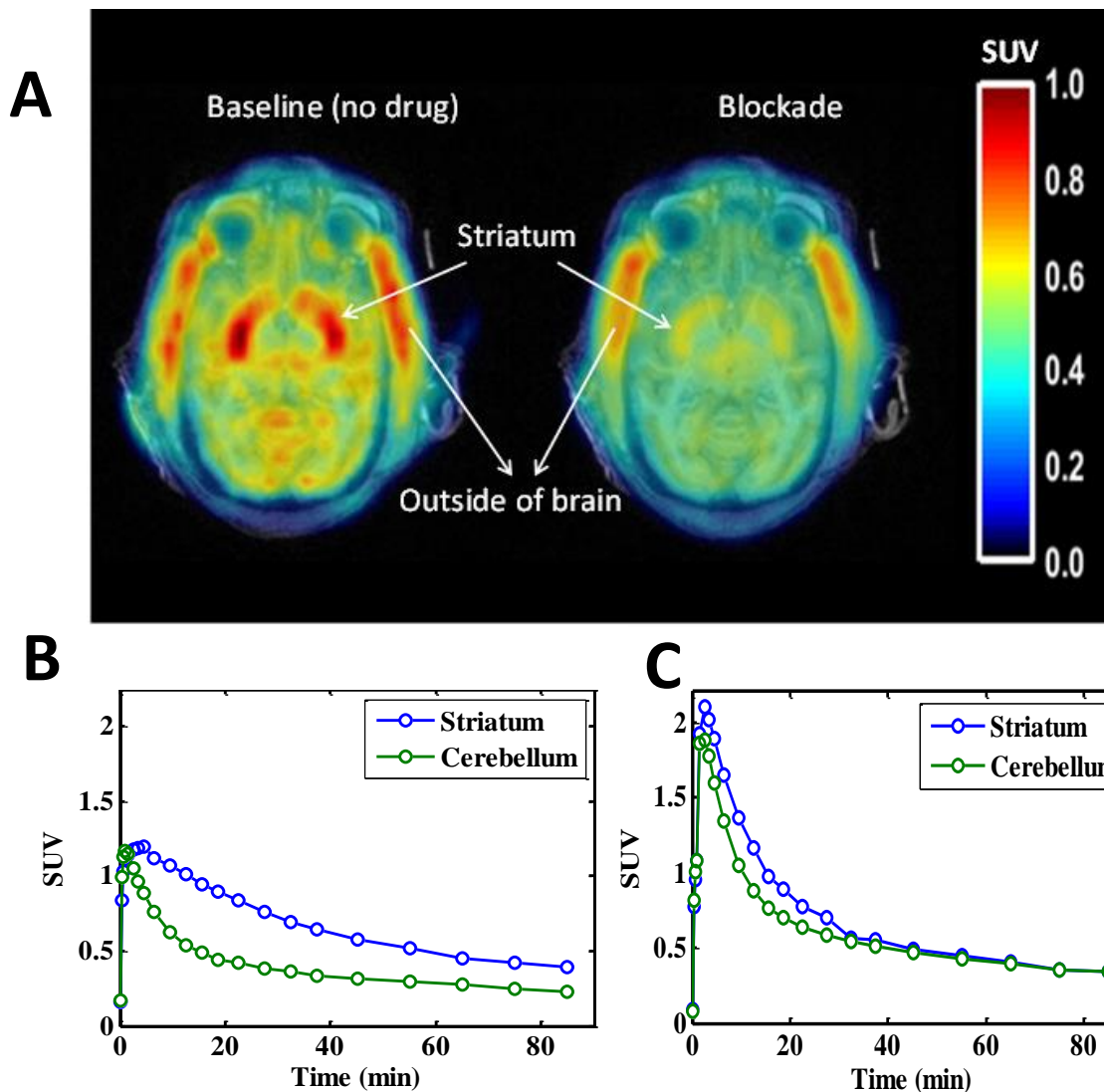


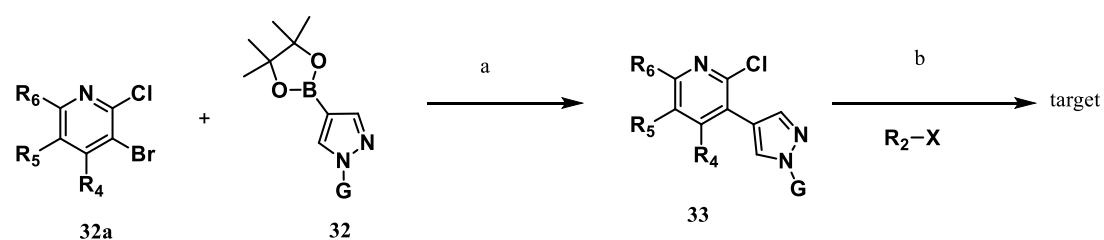
Figure 7. (A) Co-registered transverse PET/MRI summed image (0-90 min) of $[^{11}\text{C}]\mathbf{13}$ in rhesus monkey highlighting tracer uptake in the striatum. The left image $[^{11}\text{C}]\mathbf{13}$ baseline, and the right image includes blockade with compound **31**. The scale is shown in Standardized Uptake Value (SUV) units, which are normalized for the injected dose and mass of the monkey. (B) $[^{11}\text{C}]\mathbf{13}$ baseline time-activity curves. (C) $[^{11}\text{C}]\mathbf{13}$ time-activity curves under blockade with compound **31**.

CONCLUSION

In summary, a high quality M4 PAM PET tracer [^{11}C]**13** (MK-6884) was developed through optimization of binding affinity and balancing physicochemical properties of the initial lead compound. This PET tracer exhibited good brain uptake and M4-specific signal in rhesus monkey PET studies, and was used to determine plasma concentration/ receptor occupancy for M4 PAM therapeutic candidates in monkeys. Detailed information regarding plasma concentration vs M4 receptor occupancy relationship in monkey brain, as well as the clinical investigations of [^{11}C]**13**, will be the subject of future publications.

CHEMISTRY

Scheme 1. General synthetic approach to analogs.



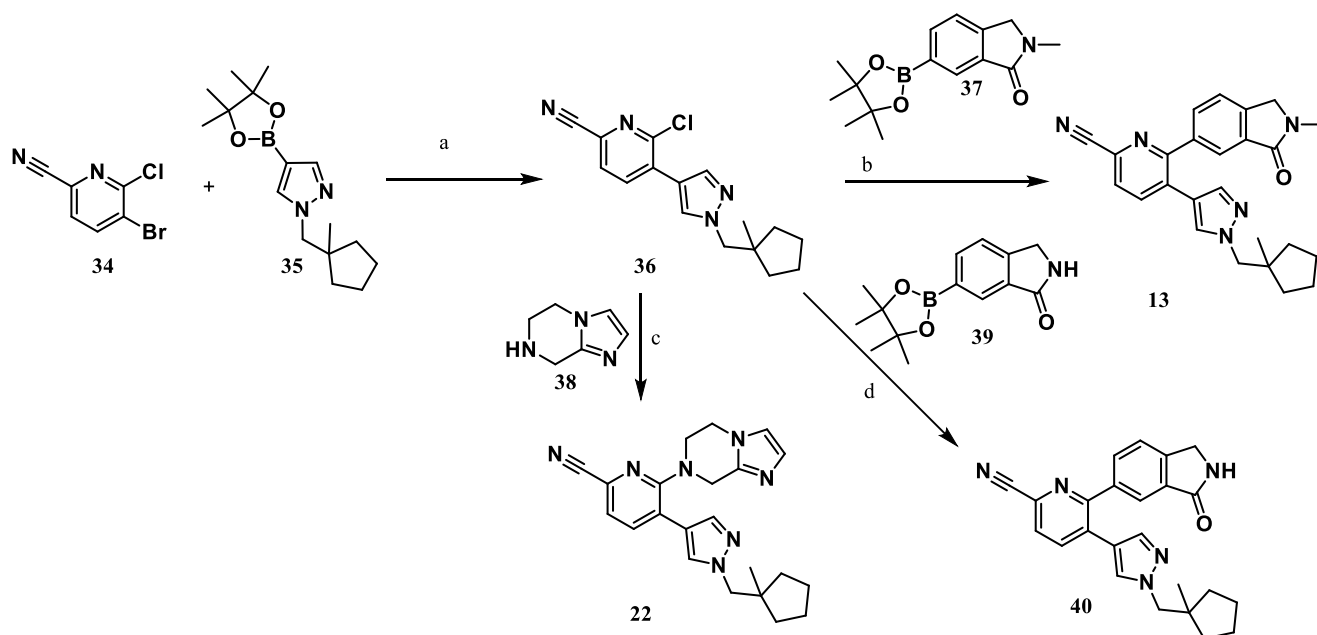
Reagents and conditions: (a) $\text{Pd}(\text{dppf})\text{Cl}_2$, K_2CO_3 , dioxane/ H_2O , 30-60°C, 3h; (b) $\text{Pd}(\text{dppf})\text{Cl}_2$, K_2CO_3 , dioxane/ H_2O , 60°C, 10 h, or NaOtBu , RuPhos Pd pre-catalyst, THF, rt, 1h.

Compounds were accessed through the generic synthetic routes outlined in references 28 and 29. A general approach is illustrated in **Scheme 1**. An appropriately substituted pyridine starting material **32a** was coupled with previously prepared pyrazole analog **32**^{28, 29} under standard Suzuki coupling conditions to afford intermediate **33**. The chlorine handle in intermediate **33** then undergoes either Suzuki coupling or C-N coupling to afford final targets.

Synthesis of compounds **13** and **22** is described in **Scheme 2**. The synthesis begins with a palladium mediated coupling under standard conditions with commercially available 5-bromo-6-

chloropicolinonitrile (**34**) and pinacol borate **35** to provide intermediate **36** in high yield. With **36** in hand, **13** is produced under palladium mediated cross-coupling with pinacol borate **37** in good yield. The [¹³C] and [³H] labelled compound **13** was obtained using compound **40** as precursor. Compound **40** was synthesized using a similar method of Suzuki cross-coupling of compound **36** with boronic ester **39** to afford the des-methyl lactam compound **40** as the labeling precursor for compound **13**. A C-N coupling with **36** and **38** catalyzed by RuPhos Pd pre-catalyst afforded compound **22**. Analogs of **13-17**, **21-25** were obtained using the same approach.

Scheme 2. Synthesis of compound **13**, **22** and **40**.

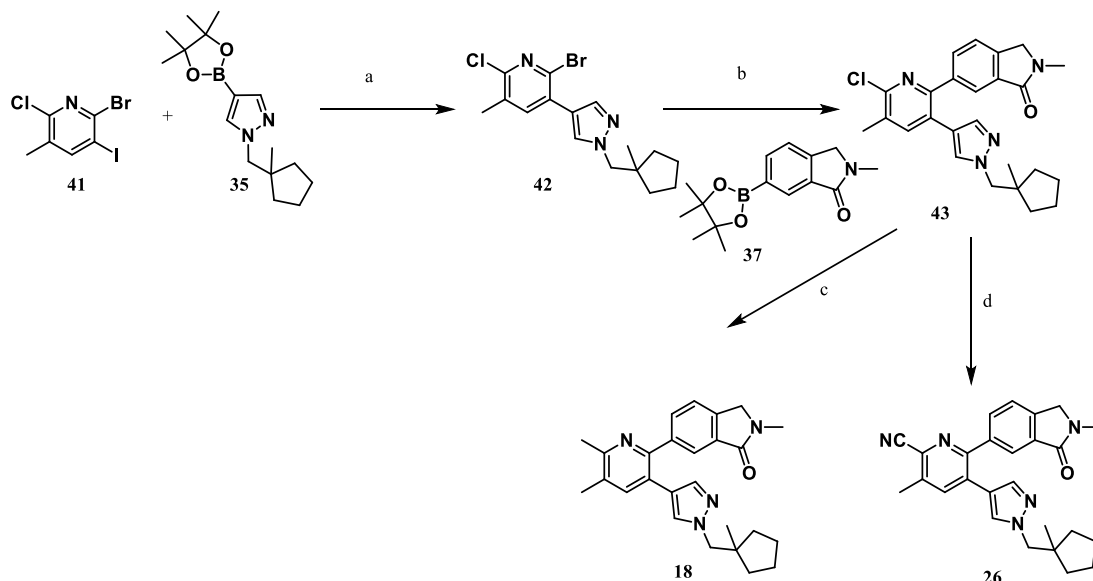


Reagents and conditions: (a) Pd(dppf)Cl₂, K₃PO₄, THF/H₂O, 50°C, 1h, 91%; (b) Pd(dppf)Cl₂, K₃PO₄, dioxane/H₂O, 60°C, 5 h, 66%; (c) NaOtBu, RuPhos Pd pre-catalyst, THF, rt, 1h, 88%, d) Pd(dtbpf)Cl₂, K₃PO₃, THF/H₂O, 60°C, 2h, 45%;

The synthesis of compounds **18** and **26** started with commercially available material **41** (**Scheme 3**). Selective palladium mediated Suzuki coupling with compound **35** gave intermediate **42**.

Another selective Suzuki coupling compound **37** afforded compound **43**. The chlorine of compound **43** was further converted to nitrile or methyl using palladium chemistry to yield compounds **18** and **26**, respectively.

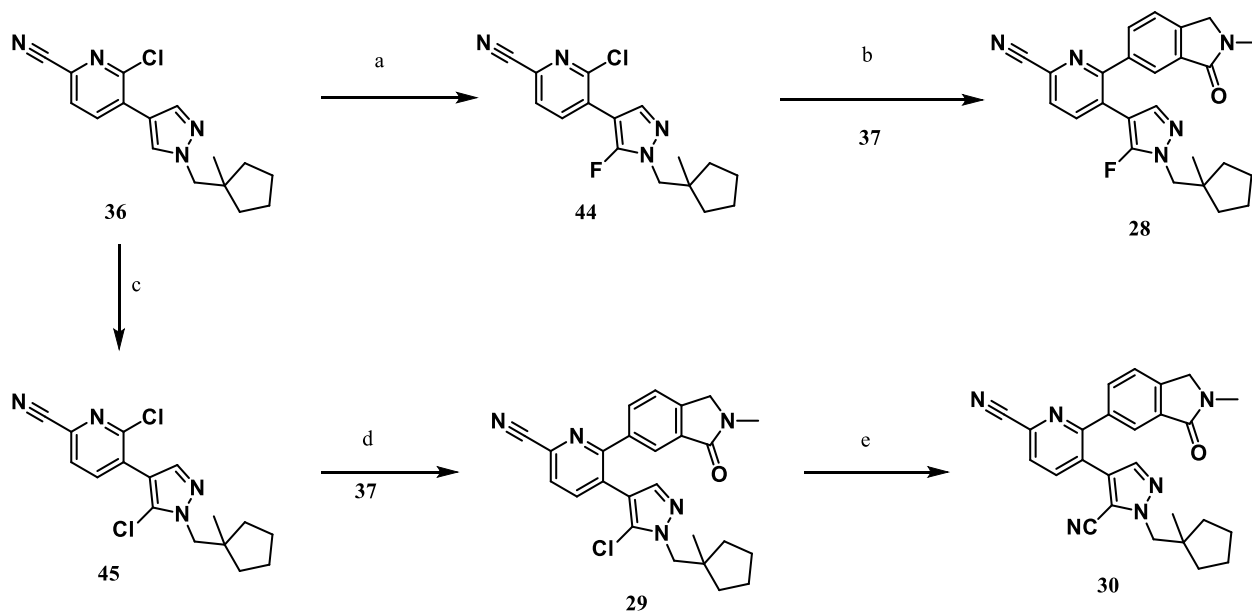
Scheme 3. Synthesis of compound **18** and **26**.



Reagents and conditions: (a) Pd(dppf)Cl₂, K₂CO₃, dioxane/H₂O, 60°C, 10 h, 66%; (b) Pd(dppf)Cl₂, K₂CO₃, dioxane/H₂O, 85°C, 10 h, 96%; (c) trimethylboroxine, Pd(dtbpf)Cl₂, K₂CO₃, dioxane/H₂O, 100°C, 2 h, 51%; (d) ZnCN₂, bis(tri-*tert*-butylphosphine)palladium(0), microwave, 180°C, 15 min., 88%.

Substituted pyrazole analogs **28-30** were synthesized by halogenation of intermediate **36** to afford chlorinated and fluorinated intermediates **44** and **45** respectively (**Scheme 4**). Further Suzuki coupling affords compounds **28** and **29**. Chloropyrazole analog **29** can be further converted to the nitrile-containing compound **30** using palladium mediated coupling with ZnCN₂.

Scheme 4. Synthesis of compounds **28-30**



Reagents and conditions: (a) SELECTFLUOR, acetonitrile, microwave, 180°C, 30 min., 14%; (b) Pd(dppf)Cl₂, K₂CO₃, dioxane/H₂O, microwave, 110°C, 1 h, 72%; (c) NCS, acetonitrile, microwave, 100°C, 30 min., 67%; (d) Pd(dppf)Cl₂, K₂CO₃, dioxane/H₂O, microwave, 115°C, 1 h, 80%; (e) ZnCN₂, Xphos Pd G2, DMF, microwave, 200°C, 30 min., 42%.

EXPERIMENTAL SECTION

Biological Evaluation

In Vitro Function Assay FLIPR assays were used to assess human M4 activity and were performed as previously reported.²⁹ CHO-K1 cells stably transfected with human M4 receptor and chimeric G-protein *Gαq15* are thawed from liquid N₂ storage, resuspended in growth medium, plated in black, clear bottom 384 well plates, and incubated 16-20 hours at 37 °C, 5% CO₂. On the day of assay, growth medium is removed, the cells are washed 2 times with wash buffer, and cells are incubated in dye loading buffer at 37 °C, 5% CO₂ for ~1 hour. Following dye loading the cell plates are placed in a FLIPR Tetra instrument and while monitoring dye fluorescence (excitation 470-495 nM/emission 515-575 nM), 10 μL of test substance at increasing concentrations is added, and fluorescence values are recorded for 4 min. Next, 10 μL of acetylcholine is added (final concentration calculated so as to achieve 20% of the maximum

acetylcholine response), and the fluorescence reading is continued for 3.5 min. In some cases, a third addition of acetylcholine (final concentration calculated to achieve 70% of the maximal acetylcholine response) is performed. Unless otherwise noted, a minimum of two independent experiments ($N \geq 2$) were performed for each compound.

FLIPR™ ACh Shift Assay

CHO-K1 cells stably transfected with human M4 receptor and chimeric G-protein Gaqi5 stably expressing a specific human, rat or rhesus muscarinic receptor subtype, were taken from LN₂ storage, thawed rapidly at 37° C, washed with CHO basal medium and dispensed in 384 well black, clear bottom plates at ~20,000 cells per well. After incubation overnight at 37° C, 5% CO₂, 95% relative humidity, the medium was removed and replaced with 25 µl per well of Calcium 5 dye buffer (Fluo-5 reagent in HBSS, 20 mM HEPES, 2.5 mM probenecid), followed by incubation at 37° C for 52 min., and subsequently 8 min. at room temperature. The plates were then loaded into the FLIPR™ instrument where 25 µl of 0.1% DMSO was added to the cells while detecting fluorescence (excitation 470-495 nm/emission 515-575 nm) for 5 min., followed by addition of 25 µl of test compound plus ACh, and continued detection of fluorescence for 5 min. For further data analysis, a max-min value was determined for each well by subtracting the minimum fluorescence signal observed immediately prior to compound addition from the maximum fluorescence signal observed in the time following compound addition.

The compounds for assay (ACh and test article) were prepared by serial, 3.16 fold dilution of 10 mM DMSO stock solutions into neat DMSO. Fifty nanoliters of the diluted ACh and 500 nL of diluted test compounds are then added to 75 µl assay buffer (HBSS, 20 mM HEPES, pH 7.4) in a

matrix fashion such that each concentration of test compound was assayed with a complete dose range of ACh.

Competition Cell Binding Assay

Competition binding of M4 allosteric analogs (in the presence of 10 μ M ACh at hM4 receptors expressed in CHO cells) were assessed with a tritium-labeled version, [3 H]**1**. Cell membranes from human M4 expressing CHO cells (CHO-hM4), suspended in assay buffer (20 mM HEPES, 100 mM NaCl, 5 mM MgCl₂, pH 7.4) at 50 μ g/ml, were combined with test article at increasing concentrations, ACh (10 μ M final concentration) and radioligand [3 H]**1** (2.2 nM final concentration) and allowed to incubate for 1.5 hour at room temperature with gentle shaking. Additional samples were also prepared to define total binding, containing DMSO (0.5% final concentration), or non-specific binding, containing compound **31** (10 μ M). Following this incubation, the samples were filtered through GF/C filter plates (that had been pre-treated with 0.3% PEI for 30 minutes) and washed 5 times with cold wash buffer (20 mM HEPES, 154 mM NaCl, pH 7.4). The filter plates were dried under vacuum for 30-60 min. at 40° C. Fifty microliters of Microscint 20 were added to each well, and the plates were read on a Topcount. Unless otherwise noted, a minimum of two independent experiments ($N \geq 2$) were performed for each compound.

Autoradiography

Autoradiography with [3 H]**1** in mouse brain slices was performed similar to previously reported methods.³³ Brain slices were incubated with [3 H]**1** (5.0 nM) at room temperature for 60 minutes (binding buffer with or without 10 μ M carbachol). Nondisplaceable binding was defined with unlabeled **1** (2 μ M). Washed and dried slides (3' x 3) were placed into a cassette against a Fuji

Imaging plate (TR2025) for 1 week at room temperature. The plate was scanned in Fujifile Life Science BAS-5000. Images were analyzed using MCID software.

In Vitro Tissue Binding Studies

In vitro tissue binding studies with [³H]**1** in rhesus monkey and human brain striatum homogenates were performed analogs to previously reported procedures.³³ Assay buffer contained 50mM Tris HCl pH 7.5, 100mM NaCl, 5mM MgCl₂, 2% DMSO, 10μM carbachol and 1:1000 mammalian protease inhibitors (P8340). Wash buffer was the same as the assay buffer without 2% DMSO and 10μM carbachol. Nondisplaceable binding was determined with unlabeled **1** (2 μM). The results were analyzed by nonlinear regression of curve fit using Prism software. The B_{max} values (in nM) of [³H]**1** calculated from assay tubes were converted to the B_{max} values using the wet tissue weight by multiplying the tissue dilution factor in the assay.

HPLC LogD

The high throughput (HT) HPLC Log D (pH 7) value is determined by the following method. The chromatographic system consists of an Agilent 1100 HPLC/DAD system and ChemStation software, both from Agilent Technologies, USA. The separations are carried out on a Poroshell 120 EC-C18 column, 30 mm x 3.0 mm I.D., 2.7 μm (Agilent Technologies, USA). The mobile phase consists of Potassium phosphate saline (10 mM Potassium phosphate, 150 mM Sodium chloride) buffered at pH 7 (mobile phase A) and acetonitrile (mobile phase B). The column oven temperature is set to 30°C and the HPLC analysis consists of a gradient. The injection volume is 5 μL and the spectrophotometric detection is set to 215, 238, and 254 nm. The chromatographic system is calibrated with a set of standards with published shake-flask Log D (pH 7) values. Linear regression is used to determine the calibration line relating the retention time to Log D for

the calibration standards. This best-fit line is then used to determine the HT HPLC Log D (pH 7) value of API (active pharmaceutical ingredient) from its measured retention time by the HPLC/DAD analysis of a solution of the API. The value was a single determination for each compound.

Chemistry.

General procedures. Reactions were conducted, purified, and analyzed according to methods widely practiced in the field, while taking necessary precautions in the exclusion of moisture and/or oxygen where appropriate. Final compounds were tested in biological assays as either TFA salts, HCl salts, or free bases. Although where relevant, the exact salt content was not determined, its mole equivalent was assumed to be equal to the number of basic moieties residing in the molecule for purposes of yield and K_i calculations. LC/MS analyses were performed on Agilent 1200 Series HPLC equipped with DAD & 6110 single quadrupole MSD & ELSD with Agilent TC-C18, 50×2.1mm, 5 μ m for acid methods, Waters X-Bridge ShieldRP18, 50×2.1mm 5 μ m for basic methods. All tested compounds exhibited $\geq 95\%$ purity under the LC conditions except for compounds **7**, **10**, **11**, **25**, **29** and **30**. UHPLC/HRMS analysis of compound **13** was performed using the following condition: LC/MS analysis was performed on a Waters Acquity UPLC system, consisting of a binary pump, a sample manager, a TUV detector and a Waters Synapt G1 Mass Spectrometer (Waters, Milford, MA) under positive or negative ESI conditions. The output signal was monitored and processed using MassLynx software designed by Waters (Milford, MA). NMR spectra were recorded on a Varian 400 MHz, 500 MHz or Bruker 400 MHz spectrometers. Residual proteo-solvent was used as internal standard for chemical shift assignments. Coupling constants are provided in Hz, with the

following spectral pattern designations: s, singlet; d, doublet; t, triplet; q, quartet; br, broad; m, multiplet, o, overlapped. IUPAC nomenclature was adopted for all final compounds and key intermediates. Compounds **1–12**, **14**, **16**, **19**, and **20** were synthesized according to previously published procedures which follows the same approach described in **Scheme 2** and conditions described **Schemes 3** and **4**.^{28, 29}

5-{1-[(1-Methylcyclopentyl)methyl]-1*H*-pyrazol-4-yl}-6-(2-methyl-3-oxo-2,3-dihydro-1*H*-isoindol-5-yl)pyridine-2-carbonitrile (13**).**

Into a 250 mL round bottom flask, purged and maintained with an inert atmosphere of nitrogen, was placed compound **35** (1.39 g, 4.8 mmol), 5-bromo-6-chloropyridine-2-carbonitrile **34** (0.87 g, 4.0 mmol), Pd(dppf)Cl₂ (156 mg, 0.24 mmol), potassium phosphate (6 mL, 2.0 N aqueous solution) and THF (25 mL). The resulting solution was stirred for 1 h at 50 °C. The reaction was then quenched by the addition of water (2 L) and was partitioned with EtOAc (3 L x 3). The combined organic layers were dried over anhydrous sodium sulfate and concentrated under reduced pressure. The residue was applied onto a silica gel column (5:1 petroleum ether:EtOAc) to yield compound **36** (1.1 g, 91%). ¹H NMR (400 MHz, CDCl₃): δ 8.00 (s, 1H), 7.92–7.94 (m, 1H), 7.86 (s, 1H), 7.64 (s, 1H), 4.09 (s, 2H), 1.42–1.74 (m, 6H), 1.38–1.42 (m, 2H), 1.01 (s, 3H). LC/MS *m/z*: [M+H]⁺ calcd for C₁₆H₁₇ClN₄, 301.12; found 301.1.

To a mixture of compound **36** (1.2 g, 3.99 mmol), compound **37** (1.1 g, 4.39 mmol), potassium phosphate (2.13 g, 7.98 mmol) was added H₂O (4 mL) and dioxane (16 mL) under an atmosphere of N₂. 1,1'-Bis(di-*tert*-butylphosphino)ferrocene palladium dichloride (584 mg, 0.80 mmol) was added and the system was purged and flushed with N₂ and it was stirred at 60 °C for 5 hr. After cooling to RT, the reaction was diluted with water and was extracted with EtOAc. The

organic was dried with anhydrous sodium sulfate and was concentrated under reduced pressure. The crude material was purified by silica gel column (0-60% 3:1 EtOAc:EtOH/hexanes) to yield the title compound **13** (1.1 g, 66%). ¹H NMR (500 MHz, DMSO-d₆): δ 8.21 (d, *J* = 5.0 Hz, 1H), 8.05 (d, *J* = 5.0 Hz, 1H), 7.65–7.60 (m, 3H), 7.38 (s, 1H), 7.32 (s, 1H), 4.52 (s, 2H), 3.86 (s, 2H), 3.09 (s, 3H), 1.46–1.58 (m, 4H), 1.36–1.40 (m, 2H), 1.10–1.14 (m, 2H), 0.75 (s, 3H). ¹³C NMR (126 MHz, DMSO-d₆): δ 167.7, 157.6, 142.5, 139.4, 138.4, 138.4, 133.2, 132.4, 132.1, 131.3, 129.9, 128.4, 123.9, 123.5, 118.1, 117.7, 60.9, 51.9, 44.1, 37.1, 29.5, 24.9, 24.2. HRMS *m/z*: [M+H]⁺ calcd for C₂₅H₂₆N₅O, 412.2137; found 412.2146.

6-(6-Fluoro-3-{1-[(1-methylcyclopentyl)methyl]-1H-pyrazol-4-yl}pyridin-2-yl)-2-methyl-2,3-dihydro-1H-isoindol-1-one (14). Compound **14** was synthesized using the same approach described in **Scheme 2**. ¹H NMR (500 MHz, DMSO-d₆) δ 8.09 (t, *J* = 8.2 Hz, 1H), 7.58 (s, 3H), 7.31 (s, 1H), 7.29 (s, 1H), 7.25 (dd, *J* = 8.4, 3.2 Hz, 1H), 4.49 (s, 2H), 3.86 (s, 2H), 3.08 (s, 3H), 1.46–1.60 (m, 4H), 1.39 (d, *J* = 6.0 Hz, 2H), 1.09–1.19 (m, 2H), 0.76 (s, 3H). LC/MS *m/z*: [M+H]⁺ calcd for C₂₄H₂₅FN₄O, 405.2; found 405.4.

6-(5-Fluoro-3-{1-[(1-methylcyclopentyl)methyl]-1H-pyrazol-4-yl}pyridin-2-yl)-2-methyl-2,3-dihydro-1H-isoindol-1-one (15). Compound **15** was synthesized using the same approach described in **Scheme 2**. ¹H NMR (500 MHz, CDCl₃) δ 8.43 (d, *J* = 2.1 Hz, 1H), 7.88 (s, 1H), 7.54 (d, *J* = 7.8 Hz, 1H), 7.51 (dd, *J* = 9.1, 2.7 Hz, 1H), 7.42 (d, *J* = 7.8 Hz, 1H), 7.29 (s, 1H), 6.89 (s, 1H), 4.40 (s, 2H), 3.85 (s, 2H), 3.20 (s, 3H), 1.51–1.71 (m, 4H), 1.42 (dt, *J* = 12.8, 6.5 Hz, 2H), 1.17–1.31 (m, 2H), 0.82 (s, 3H). LC/MS *m/z*: [M+H]⁺ calcd for C₂₄H₂₅FN₄O, 405.2; found 405.2.

3-{1-[(1-Methylcyclopentyl)methyl]-1*H*-pyrazol-4-yl}-2-(2-methyl-3-oxo-2,3-dihydro-1*H*-isoindol-5-yl)pyridine-4-carbonitrile (16). Compound **16** was synthesized using the same approach described in **Scheme 2**. ¹H NMR (500 MHz, DMSO-*d*₆) δ 8.82 (d, *J* = 5.0 Hz, 1H), 7.95 (d, *J* = 5.0 Hz, 1H), 7.49–7.64 (m, 4H), 7.37 (s, 1H), 4.45 (s, 2H), 3.93 (s, 2H), 3.06 (s, 3H), 1.46–1.63 (m, 4H), 1.39 (d, *J* = 5.8 Hz, 2H), 1.07–1.21 (m, 2H), 0.74 (s, 3H). LC/MS *m/z*: [M+H]⁺ calcd for C₂₅H₂₅N₅O, 412.2; found 412.4.

6-(6-Fluoro-5-methyl-3-{1-[(1-methylcyclopentyl)methyl]-1*H*-pyrazol-4-yl}pyridin-2-yl)-2-methyl-2,3-dihydro-1*H*-isoindol-1-one (17). Compound **17** was synthesized using the same approach described in **Scheme 2**. ¹H NMR (400 MHz, MeOD) δ 7.90 (d, *J* = 9.2 Hz, 1H), 7.70 (s, 1H), 7.54–7.64 (m, 2H), 7.33 (s, 1H), 7.16 (s, 1H), 4.52 (s, 2H), 3.89 (s, 2H), 3.19 (s, 3H), 2.37 (s, 3H), 1.58–1.60 (m, 2H), 1.38–1.50 (m, 2H), 1.25–1.31 (m, 2H), 1.13–1.22 (m, 2H), 0.79 (s, 3H). LC/MS *m/z*: [M+H]⁺ calcd for C₂₅H₂₇FN₄O, 419.2; found 419.1.

6-(5,6-Dimethyl-3-{1-[(1-methylcyclopentyl)methyl]-1*H*-pyrazol-4-yl}pyridin-2-yl)-2-methyl-2,3-dihydro-1*H*-isoindol-1-one (18).

Compound **35** (288 mg, 0.993 mmol), 2-bromo-6-chloro-3-iodo-5-methylpyridine (**41**) (300 mg, 0.903 mmol), 1,1'-bis(diphenylphosphino)ferrocene-palladium(ii)dichloride dichloromethane complex (73.7 mg, 0.090 mmol) and potassium carbonate (2.71 ml, 2.71 mmol) were charged in a reaction vessel with Dioxane (5 ml). The mixture was de-gassed three times before it was

heated to 60°C for 10 hr. The reaction mixture was worked up and concentrated to dryness and purified with ISCO eluted with EtOAc in Hex 0% to 40% to afford compound **42** (220 mg, 66%).

Compound **42** (120 mg, 0.325 mmol), compound **37** (89 mg, 0.325 mmol), 1,1'-bis(diphenylphosphino)ferrocene-palladium(ii)dichloride dichloromethane complex (26.6 mg, 0.033 mmol) and potassium carbonate (0.976 ml, 0.976 mmol) were charged in a reaction vessel with dioxane (5 ml). The mixture was de-gassed three times before it was heated to 85 °C for 10 hr. LCMS showed mostly product. The reaction mixture was worked up and concentrated to dryness and purified with ISCO column (24 g) eluted with EtOA in Hex 50% to 100% to give compound **43** (136 mg, 96 %).

2,4,6-Trimethyl-1,3,5,2,4,6-trioxatriborinane (6.93 mg, 0.055 mmol), compound **43** (20 mg, 0.046 mmol) and 1,1'-bis(di-*tert*-butylphosphino)ferrocene palladium dichloride (3.00 mg, 4.60 μmol) were placed in a 4 mL reaction vial and evacuated and charged with nitrogen. 1,4-Dioxane (1 mL) and potassium (3 M in water, 0.138 mL, 0.138 mmol) were added to the sealed vial and the system was heated to 100 °C. After 2 h, the crude reaction mixture was cooled and purified by mass triggered reverse phase HPLC (ACN/water with 0.1% NH₄OH modifier) to afford compound **18** (9.8 mg, 51%). ¹H NMR (500 MHz, CDCl₃): δ 7.9 (s, 1H), 7.6 (d, *J* = 8.6 Hz, 1H), 7.57 (s, 1H), 7.4 (d, *J* = 7.8 Hz, 1H), 7.3 (s, 1H), 6.86 (s, 1H), 4.4 (s, 2H), 3.86 (s, 2H), 3.23 (s, 2H), 2.6 (s, 2H), 2.4 (s, 2H), 1.60–1.73 (m, 4H), 1.40–1.50 (m, 2H), 1.20–1.30 (m, 2H), 0.85 (s, 2H). LC/MS *m/z*: [M+H]⁺ calcd for C₂₆H₃₀N₄O, 415.3; found 415.3.

6-[5-Fluoro-6-(fluoromethyl)-3-{1-[(1-methylcyclopentyl)methyl]-1*H*-pyrazol-4-yl}pyridin-2-yl]-2-methyl-2,3-dihydro-1*H*-isoindol-1-one (19). Compound **19** was synthesized using the

same approach described in **Scheme 2**. ^1H NMR (500 MHz, CDCl_3) δ 7.91 (s, 1H), 7.52–7.61 (m, 2H), 7.42 (d, $J = 7.7$ Hz, 1H), 7.30 (s, 1H), 6.89 (s, 1H), 5.57 (d, $J = 47.5$ Hz, 2H), 4.40 (s, 2H), 3.85 (s, 2H), 3.21 (s, 3H), 1.51–1.71 (m, 4H), 1.42 (dt, $J = 12.5, 6.3$ Hz, 2H), 1.25 (d, $J = 7.5$ Hz, 2H), 0.82 (s, 3H). LC/MS m/z : $[\text{M}+\text{H}]^+$ calcd for $\text{C}_{25}\text{H}_{26}\text{F}_2\text{N}_4\text{O}$, 437.2; found 437.0.

3-{1-[(1-Methylcyclopentyl)methyl]-1*H*-pyrazol-4-yl}-2-(2-methyl-3-oxo-2,3-dihydro-1*H*-isoindol-5-yl)-5,6-dihydro-7*H*-cyclopenta[*b*]pyridin-7-one (20). Compound **20** was synthesized using the same approach describe in **Scheme 2**. ^1H NMR (400MHz, MeOD) δ 8.18 (s, 1H) 7.61–7.70 (m, 3H), 7.43 (s, 1H), 7.12 (s, 1H), 4.53 (s, 2H), 3.86 (s, 2H), 3.22–3.27 (m, 2H), 3.18 (s, 3H), 2.76–2.83 (m, 2H), 1.66–1.77 (m, 2H), 1.58 (d, $J = 8.2$ Hz, 2H), 1.43 (dd, $J = 14.9, 7.4$ Hz, 2H), 1.11–1.20 (m, 2H), 0.76 (s, 3H). LC/MS m/z : $[\text{M}+\text{H}]^+$ calcd for $\text{C}_{27}\text{H}_{28}\text{N}_4\text{O}_2$, 441.2; found 441.2.

6-(Imidazo[1,2-*a*]pyridin-7-yl)-5-{1-[(1-methylcyclopentyl)methyl]-1*H*-pyrazol-4-yl}pyridine-2-carbonitrile (21). Compound **21** was synthesized using the same approach described in **Scheme 2**. ^1H NMR (400MHz, MeOD) δ 8.80 (d, $J = 6.8$ Hz, 1H), 8.28 (s, 1H), 8.21 (d, $J = 8.4$ Hz, 1H), 8.11(s, 1H), 8.09 (s, 1H), 8.00 (d, $J = 8.0$ Hz, 1H), 7.61 (s, 1H), 7.54 (s, 1H), 7.48 (d, $J = 6.8$ Hz, 1H), 3.96 (s, 2H), 1.45–1.70 (m, 6H), 1.20–1.30 (m, 2H), 0.84 (s, 3H). LC/MS m/z : $[\text{M}+\text{H}]^+$ calcd for $\text{C}_{23}\text{H}_{22}\text{N}_6$, 383.2; found 383.2

6-(5,6-Dihydroimidazo[1,2-*a*]pyrazin-7(8*H*)-yl)-5-{1-[(1-methylcyclopentyl)methyl]-1*H*-pyrazol-4-yl}pyridine-2-carbonitrile (22).

To a suspension of compound **36** (20 mg, 0.066 mmol), compound **38** (12 mg, 0.1 mmol) in THF (332 μ L) under N₂ was added RuPhos Pd pre-catalyst (4.85 mg, 6.7 μ mol) and sodium tert-butoxide (133 μ L, 2.0 N THF solution, 0.27 mmol). The mixture was stirred at room temperature for 1 h. The reaction was diluted with EtOAc (3 mL). The organic layer was removed and the aqueous layer was further extracted with EtOAc (2x3 mL). The combined organic layer was washed with brine, and dried using anhydrous Na₂SO₄. QuardraPure was added and stirred at rt for 1 hr to remove Pd. The solution was then filtered and concentrated to dryness under reduced pressure. The crude material was purified by Gilson reverse phase HPLC using Sunfire C18 (19x150 mm column), mobile phase A, 0.1% TFA in H₂O, mobile phase B, 0.1% TFA in acetonitrile, gradient, 15-75% B, 20 mins run. Compound **22** (28 mg, 88%). ¹H NMR (500 MHz, DMSO-d₆) δ 8.36 (s, 1H), 8.04–8.11 (m, 2H), 7.76 (d, *J* = 7.8 Hz, 1H), 7.67 (s, 2H), 4.67 (s, 2H), 4.11 (d, *J* = 5.1 Hz, 2H), 4.06 (s, 2H), 3.64 (d, *J* = 5.0 Hz, 2H), 1.61 (s, 6H), 1.28 (s, 2H), 0.92 (s, 3H). LC/MS *m/z*: [M+H]⁺ calcd for C₂₂H₂₅N₇, 388.2; found 388.3.

6-(2-Bromo-5,6-dihydroimidazo[1,2-*a*]pyrazin-7(8*H*)-yl)-5-{1-[(1-methylcyclopentyl)methyl]-1*H*-pyrazol-4-yl}pyridine-2-carbonitrile (23). Compound **23** was synthesized using the same approach described in **Scheme 2**. ¹H NMR (500 MHz, DMSO-d₆) δ 8.26 (s, 1H), 7.93–8.03 (m, 2H), 7.69 (d, *J* = 7.7 Hz, 1H), 7.28 (s, 1H), 4.26 (s, 2H), 4.04 (s, 2H), ~3.4–4.0 (m, 2H), 1.59 (s, 6H), 1.25 (s, 2H), 0.90 (s, 3H). LC/MS *m/z*: [M+H]⁺ calcd for C₂₂H₂₄BrN₇, 466.1; found 468.3.

6-[4-(3-Methylazetid-1-yl)piperidin-1-yl]-5-{1-[(1-methylcyclopentyl)methyl]-1*H*-pyrazol-4-yl}pyridine-2-carbonitrile (24). Compound **24** was synthesized using the same approach

described in **Scheme 2**. ^1H NMR (500 MHz, DMSO- d_6) δ 8.24 (s, 1H), 7.99 (s, 1H), 7.94 (d, J = 7.7 Hz, 1H), 7.63 (d, J = 7.7 Hz, 1H), 4.00–4.31 (m, 4H), 3.61–3.85 (m, 2H), 3.47–3.59 (m, 2H), 2.83 (s, 1H), 2.71 (t, J = 12.1 Hz, 2H), 1.85–1.97 (m, 2H), 1.55–1.72 (m, 6H), 1.38–1.51 (m, 2H), 1.23–1.36 (m, 4H), 1.10–1.20 (m, 2H), 0.93 (s, 3H). LC/MS m/z : $[\text{M}+\text{H}]^+$ calcd for $\text{C}_{25}\text{H}_{34}\text{N}_6$, 419.3; found 419.5.

6-(5,6-Dihydro[1,2,4]triazolo[4,3-*a*]pyrazin-7(8*H*)-yl)-5-{1-[(1-methylcyclopentyl)methyl]-1*H*-pyrazol-4-yl}pyridine-2-carbonitrile (25). Compound **25** was synthesized using the same approach described in **Scheme 2**. ^1H NMR (500 MHz, DMSO- d_6) δ 8.48 (s, 1H), 8.29 (s, 1H), 8.01 (d, J = 7.7 Hz, 1H), 7.98 (s, 1H), 7.70 (d, J = 7.7 Hz, 1H), 4.46 (s, 2H), 4.08–4.13 (m, 2H), 4.05 (s, 2H), 3.52–3.63 (m, 2H), 1.60 (s, 6H), 1.26 (s, 2H), 0.91 (s, 3H). LC/MS m/z : $[\text{M}+\text{H}]^+$ calcd for $\text{C}_{21}\text{H}_{24}\text{N}_8$, 389.2; found 389.5.

3-Methyl-5-{1-[(1-methylcyclopentyl)methyl]-1*H*-pyrazol-4-yl}-6-(2-methyl-3-oxo-2,3-dihydro-1*H*-isoindol-5-yl)pyridine-2-carbonitrile (26)

Compound **43** (70 mg, 0.161 mmol), bis(*tri-tert*-butylphosphine)palladium(0) (8.22 mg, 0.016 mmol) and zinc cyanide (0.020 mL, 0.322 mmol) were dissolved in dioxane (1.5 mL) in a sealed tube. The reaction was heated at 180 °C under microwave irradiation for 15 min and the mixture was filtered and the solvent was removed under reduced pressure. The residue was dissolved in EtOAc and washed with aqueous saturated NaHCO_3 , water, and brine. The organic layer was dried over anhydrous Na_2SO_4 , filtered and concentrated. The material was purified by silica gel chromatography (5-100% EtOAc/hexanes) to give compound **26** (60 mg, 88%). ^1H NMR (500 MHz, CDCl_3): δ 7.90 (s, 1H), 7.75 (s, 1H), 7.62 (d, J = 6.5 Hz, 1H), 7.49 (d, J = 8.0 Hz, 1H),

7.39 (s, 1H), 6.94 (s, 1H), 4.45 (s, 2H), 3.90 (s, 2H), 3.24 (s, 3H), 2.66 (s, 3H), 1.20–1.80 (m, 8H), 0.85 (s, 3H). LC/MS m/z : $[M+H]^+$ calcd for C₂₆H₂₇N₅O, 426.2; found 426.0.

3-Chloro-5-{1-[(1-methylcyclopentyl)methyl]-1*H*-pyrazol-4-yl}-6-(2-methyl-3-oxo-2,3-dihydro-1*H*-isoindol-5-yl)pyridine-2-carbonitrile (27). Compound **27** was synthesized using the same approach described in **Scheme 3**. Compound **27** was synthesized using the same approach described in **Scheme 3**. ¹H NMR (400MHz, MeOD) δ 8.29 (s, 1H), 7.76 (s, 1H), 7.65–7.70 (m, 2H), 7.46 (s, 1H), 7.26 (s, 1H), 4.58 (s, 2H), 3.91 (s, 2H), 3.22 (s, 3H), 1.55–1.70 (m, 4H), 1.40–1.50 (m, 2H), 1.15–1.25 (m, 2H), 0.82 (s, 3H). LC/MS m/z : $[M+H]^+$ calcd for C₂₅H₂₄ClN₅O, 446.2; found 446.1.

5-{5-Fluoro-1-[(1-methylcyclopentyl)methyl]-1*H*-pyrazol-4-yl}-6-(2-methyl-3-oxo-2,3-dihydro-1*H*-isoindol-5-yl)pyridine-2-carbonitrile (28)

Selectfluor (402 mg, 1.13 mmol) was added to a mixture of compound **36** (310 mg, 1.03 mmol) in acetonitrile (5 ml) and the mixture was stirred at 180°C under microwave irradiation for 30 min. After cooling, the reaction mixture was concentrated. The residue was purified by column chromatography on silica gel (ISCO 40 g gold), eluting with EtOAc/isoohexane (2/1) to compound **44** (50 mg, 14% yield). LC/MS m/z : $[M+H]^+$ calcd for C₁₆H₁₆ClFN₄, 319.1; found 319.0.

A mixture of potassium phosphate tribasic (30.0 mg, 0.14 mmol), [1,1'-bis(diphenylphosphino)ferrocene]dichloropalladium(II) (1.9 mg, 2.4 μmol), compound **44** (15 mg, 0.047 mmol) and compound **37** (19.0 mg, 0.071 mmol) in 1,4-dioxane (2 ml) and water (0.25 ml) was degassed and purged with N₂ 7 times and the mixture was stirred at 110 °C under

microwave irradiation for 1h. The reaction mixture was concentrated to dryness. The residue was purified by column chromatography on silica gel (ISCO gold 40g), eluting with (hex/EA 1/2)) to give compound **28** (14.5 mg, 72%). ¹H NMR (500 MHz, CDCl₃) δ 7.86–7.93 (m, 2H), 7.70 (d, *J* = 8.0 Hz, 1H), 7.67 (dd, *J* = 7.8, 1.6 Hz, 1H), 7.47 (d, *J* = 7.8 Hz, 1H), 7.02 (d, *J* = 2.9 Hz, 1H), 4.40 (s, 2H), 3.80 (s, 2H), 3.20 (s, 3H), 1.56–1.70 (m, 4H), 1.45–1.54 (m, 2H), 1.25–1.34 (m, 2H), 0.89 (s, 3H). LC/MS *m/z*: [M+H]⁺ calcd for C₂₅H₂₄FN₅O, 430.2; found 430.1.

5-{5-Chloro-1-[(1-methylcyclopentyl)methyl]-1*H*-pyrazol-4-yl}-6-(2-methyl-3-oxo-2,3-dihydro-1*H*-isoindol-5-yl)pyridine-2-carbonitrile (29**)**

A mixture of NCS (98 mg, 0.73 mmol) and compound **36** (200 mg, 0.67 mmol) in acetonitrile (4 ml) was stirred at 100°C under microwave irradiation for 30 min. The reaction mixture was concentrated. The residue was purified by column chromatography on silica gel (ISCO gold 80 g), eluting with EtOAc/isohehexane (15/1) to compound **45** (150 mg, 0.45 mmol, 67 %) as a colorless oil.

A mixture of potassium phosphate tribasic (57.0 mg, 0.268 mmol), [1,1'-bis(diphenylphosphino)ferrocene]dichloropalladium(II) (3.65 mg, 4.47 μmol), compound **45** (30 mg, 0.089 mmol) and compound **37** (36.7 mg, 0.13 mmol) in 1,4-dioxane (2 ml) and water (0.25 ml) was degassed and purged with N₂ 7 times and the mixture was stirred at 110 °C under microwave irradiation for 1h. The reaction mixture was concentrated. The residue was purified by column chromatography on silica gel (ISCO gold 40g), eluting with (hex/EA 1/2)) to give compound **29** (32 mg, 80 %). ¹H NMR (500 MHz, CDCl₃) δ 7.92 (d, *J* = 7.9 Hz, 1H), 7.85 (s, 1H), 7.72 (d, *J* = 7.9 Hz, 1H), 7.60 (dd, *J* = 7.8, 1.5 Hz, 1H), 7.40 (d, *J* = 7.8 Hz, 1H), 7.21 (s, 1H), 4.38 (s, 2H), 3.98 (s, 2H), 3.19 (s, 3H), 1.51–1.74 (m, 6H), 1.27–1.37 (m, 2H), 0.90 (s, 3H). LC/MS *m/z*: [M+H]⁺ calcd for C₂₅H₂₄ClN₅O, 446.2; found 446.3.

5-{5-Cyano-1-[(1-methylcyclopentyl)methyl]-1*H*-pyrazol-4-yl}-6-(2-methyl-3-oxo-2,3-dihydro-1*H*-isoindol-5-yl)pyridine-2-carbonitrile (30)

A mixture of compound **29** (11.4 mg, 0.026 mmol), dicyanozinc (9.0 mg, 0.077 mmol) and chloro(2-dicyclohexylphosphino-2',4',6'-triisopropyl-1,1'-biphenyl)[2-(2'-amino-1,1'-biphenyl)]palladium(II) (2.011 mg, 2.56 μ mol) in DMF (4 mL) was heated to 200 °C under microwave irradiation for 30 min. The crude reaction was concentrated and directly purified by column chromatography on silica gel (20:1 CH₂Cl₂/MeOH) to afford compound **30** (4.7 mg, 42%). MS: 437 (M+1). ¹H NMR (500 MHz, CDCl₃): δ 8.01 (d, *J* = 7.5 Hz, 1H), 7.80 (d, *J* = 8.0 Hz, 1H), 7.76 (dd, *J* = 7.5, 1.5 Hz, 1H), 7.73 (s, 1H), 7.54 (d, *J* = 8.0 Hz, 1H), 7.62 (dd, *J* = 8.0, 1.5 Hz, 1H), 7.30 (s, 1H), 4.44 (s, 2H), 4.16 (s, 2H), 3.22 (s, 3H), 1.27–1.73 (m, 8 H), 0.95 (s, 3H). LC/MS *m/z*: [M+H]⁺ calcd for C₂₅H₂₄FN₅O, 437.2; found 437.4.

5-{1-[(1-Methylcyclopentyl)methyl]-1*H*-pyrazol-4-yl}-6-(3-oxo-2,3-dihydro-1*H*-isoindol-5-yl)pyridine-2-carbonitrile (40)

Compound **36** (60 mg, 0.2 mmol), compound **39** (62 mg, 0.24 mmol), (1,1'-bis(di-tert-butylphosphino)ferrocene palladium dichloride (10.42 mg, 0.016 mmol) and potassium phosphate tribasic (300 μ l, 2 N aq. solution, 0.6 mmol) solution were added to a reaction tube with THF (1 mL). The mixture was degassed three times before it was heated to 60 °C for 5 hr. After cooling, the reaction mixture was quenched by the addition of water (3 mL) and was partitioned with EtOAc (3 mL x 3). The combined organic layers were dried over anhydrous sodium sulfate and concentrated under reduced pressure. The crude material was purified with reverse phase HPLC, flow rate 50 mL/min using Sunfire C18 (19x150 mm column), mobile phase A, 0.1% NH₄OH in H₂O, mobile phase B, 0.1% NH₄OH in acetonitrile, gradient, 16% to

56% B, 25 mins run. Compound **40** (33 mg, 0.083 mmol, 45 %). ^1H NMR (500 MHz, DMSO- d_6): δ 8.63 (s, 1H), 8.21 (d, $J = 5.0$ Hz, 1H), 8.05 (d, $J = 5.0$ Hz, 1H), 7.60–7.65 (m, 3H), 7.39 (s, 1H), 7.32 (s, 1H), 4.43 (s, 2H), 3.86 (s, 2H), 1.46–1.57 (m, 4H), 1.37–1.41 (m, 2H), 1.10–1.15 (m, 2H), 0.75 (s, 3H). ^{13}C NMR (126 MHz, DMSO- d_6): δ 169.9, 157.6, 144.9, 139.3, 138.4, 138.4, 133.4, 132.5, 132.1, 131.3, 130.0, 128.4, 124.4, 123.8, 118.1, 117.7, 60.9, 45.4, 44.1, 37.1, 24.9, 24.2. HRMS m/z : $[\text{M}+\text{H}]^+$ calcd for $\text{C}_{24}\text{H}_{23}\text{N}_5\text{O}$, 398.1981; found 398.1973.

General Radiochemical Methods

Detailed radiochemistry for labeled compounds will be described in a future publication.

Briefly, a Siemens RDS-111 cyclotron was used to produce $^{11}\text{C}[\text{CO}_2]$ by the $^{14}\text{N}(p,\alpha)^{11}\text{C}$ reaction produced at PETNET Solutions (North Wales, PA). The resulting $^{11}\text{C}[\text{CO}_2]$ was converted to ^{11}C iodomethane ($^{11}\text{C}[\text{CH}_3\text{I}]$) using a TRACERlab FXc (GE Healthcare, Wauwatosa, WI). For all ^{11}C cyanation reactions, the $^{11}\text{C}[\text{CO}_2]$ was converted to $^{11}\text{C}[\text{HCN}]$ using an Eckert & Ziegler Modular Lab apparatus (Berlin, Germany). Briefly, $^{11}\text{C}[\text{CO}_2]$ (1,500 mCi) from the target was trapped on molecular sieves at room temperature. The $^{11}\text{C}[\text{CO}_2]$ was released and mixed with hydrogen gas at 350 °C then passed through a preheated nickel oven at 420 °C for conversion to $^{11}\text{C}[\text{CH}_4]$. The $^{11}\text{C}[\text{CH}_4]$ gas was purified by passing it through Ascarite and Sicapent columns to remove water and unreacted $^{11}\text{C}[\text{CO}_2]$. The $^{11}\text{C}[\text{CH}_4]$ was mixed with anhydrous ammonia and passed through a high temperature (950 °C) platinum oven, resulting in the formation of $^{11}\text{C}[\text{HCN}]$ (non-decay corrected radiochemical yields of 700-1000 mCi). Precursors were prepared at the Research Laboratories of Merck & Co., Inc. (Rahway, NJ, USA). The semi-automated radiosynthesis of ^{11}C compounds were performed with a 233XL liquid handler (Gilson Inc., Middleton, WI) in a lead-shielded fume hood. The identity, specific activity, and

radiochemical purity of [^{11}C] compounds were determined using a Waters 600E HPLC, a Waters 996 ultraviolet (PDA) detector (Waters, Milford, MA), and a FlowCount photodiode radio detector (Bioscan Inc., Washington D.C.). A Waters Xbridge C18 column (4.6x150 mm, 5 μm) with a mobile phase of acetonitrile and water. The products were purified using a Gemini C-18 HPLC column (Phenomex, Torrance, CA) at a flow rate of 5 mL/min.

Radiochemical Synthesis of [^{11}C] Compounds

Unless otherwise noted, this procedure was used for all [^{11}C]CH₃I reactions. [^{11}C]MeI (13 GBq) was trapped in a 0°C mixture of precursor (0.2 mg, ~ 1 μmol) in dimethylformamide (0.2 mL) and sodium hydroxide (1 μL , 5 M). This mixture was transferred to a 2 mL v-vial preheated to 50°C. The reaction mixture was heated at 50°C for 4 minutes, diluted with H₂O (0.8 ml) and purified by HPLC (Phenomenex Gemini C18, 5 μm , 100A, 10 \times 150 mm) using 45:55 acetonitrile:10 mM sodium phosphate at 5 mL/min, 20 mins run. The HPLC fraction containing [^{11}C] compound (~ retention time ~10.2 min for [^{11}C]**2**, ~12.1 min for [^{11}C]**13**) was collected in a sterile glass vial. [^{11}C]**22** was synthesized by reaction of [^{11}C]HCN (18 GBq) with bromo precursor **22** (1 mg, 2.27 μmol), triphenylphosphine palladium (2.4 mg, 2.0 μmol) and potassium bicarbonate (6 mg, 60 μmol) in an auto-sampler vial in dimethylformamide (0.3 ml) at 120 °C for 5 min. Subsequently, after cooling the crude reaction mixture to room temperature, 0.8 ml 10 mM sodium phosphate was added, and the reaction mixture was purified by using the semi-preparative HPLC method described above, Phenomenex Gemini C18 column (10x150 mm ,5 μm), using 42:58 acetonitrile:10 mM sodium phosphate at 5 mL/min, 30 mins run. The peak corresponding to [^{11}C]**22** with retention time ~13.5 min was collected, diluted with saline and transferred to a sterile capped vial to provide [^{11}C]**22** injection solution. The final product was

tested for chemical and radiochemical purity by means of an analytical HPLC system (Waters) using a Xbridge Phenyl 3.5 μ 4.6x150 mm column at a flow rate of 1 mL/min. For [^{11}C]2, the mobile phase increased from 35:65 to 60:40 acetonitrile/ Na_2HPO_4 (10 mM) using a 15-min linear gradient. [^{11}C]13 and [^{11}C]22, the mobile phase was acetonitrile / Na_2HPO_4 (10mM): 42/58. Confirmation of the identity of the product was determined by coinjection of a sample of compound 2, or 13, or 22, and radiochemical purity (>98%) was determined using a sodium iodide detector (Bioscan). The retention times for compound [^{11}C]2, [^{11}C]13 and [^{11}C]22 were 10.3, 9.7, 9.9 min, respectively.

In Vivo PET Imaging Studies in Rhesus Monkey

The Research Laboratories of Merck & Co., Inc. obtained rhesus monkeys from Covance Inc. (Alice, TX), New Iberia Research Center (New Iberia, LA) and Mannheimer Foundation (Homestead, FL). All monkey PET imaging studies were conducted under the guiding principles of the American Physiological Society and the Guide for the Care and Use of Laboratory Animals published by the US National Institutes of Health (NIH publication No 85-23, revised 2010) and were approved by the Research Laboratories of Merck & Co., Inc. (West Point, PA USA). Five rhesus monkeys (age range 5-9, ~ 7-10 kg, 2 males and 3 females) were initially sedated with ketamine (10 mg/kg, IM), then induced with propofol (5 mg/kg, IV), intubated, and respired with medical grade air and oxygen mixture at ~10 ml.breath $^{-1}$ kg $^{-1}$ and 23 respirations per minute. The anesthesia was maintained with propofol (0.4-0.55 mg.kg $^{-1}$.min $^{-1}$) for the duration of the study. Body temperature was maintained with circulating water heating pads, and temperature, oxygen saturation, blood pressure, and end-tidal CO $_2$ were monitored for the

duration of the study. Dynamic PET scans were acquired by Imaging laboratory at the Research Laboratories of Merck & Co., Inc. (West Point, PA, USA) in PET/CT or HR+ scanner (Siemens) for 90 min following a 2-min bolus IV injection of [^{11}C]compound (~ 185 MBq, < 2 μg). Frame durations were ranged from 15 s to 10 min. PET images were corrected for attenuation and scatter. PET scans were co-registered to standard template space with or without subject/template MRI to define the regional uptake. Regional time activity curves were drawn on the PET images to quantify the regional tracer uptake in terms of peak standard uptake value (SUV), area under the curve (AUC) or SUV ratio of target and reference regions. Based on prior autoradiography and saturation binding studies cerebellum has minimal M4 receptors, and therefore cerebellum was used as reference region for simplified reference tissue model (SRTM). Appropriate kinetic modeling was applied to obtain nondisplaceable binding potential (BP_{ND}).

ASSOCIATED CONTENT

Supporting Information. ^1H NMR and LCMS spectra of final compounds; molecular formula strings and biological data. This material is available free of charge via the Internet at <http://pubs.acs.org>.

AUTHOR INFORMATION

Corresponding Author

*Phone: 215-652-7291. E-mail: ling.tong@merck.com

Notes

The authors are employees of Merck Sharp & Dohme Corp., a subsidiary of Merck & Co., Inc., Kenilworth, NJ, USA (MSD) except for X.G., J.M.W., A.J., C.S., M.E., Z.M., B.H., R.G., S.T.H., P.M., J.M., F.T., F.J.M., M.D.S., S.R. D.H. who were employed at MSD during this work.

ACKNOWLEDGMENTS

The authors would like to thank Dorothy Levorse and Dina Zhang for obtaining HPLC Log D values.

ABBREVIATIONS

mAChR, muscarinic acetylcholine receptors; ACh, acetylcholine; BP_{ND}, nondisplaceable binding potential; M4, muscarinic acetylcholine receptor 4; FLIPR, Fluorescent Imaging Plate Reader assay; RO, receptor occupancy; sF Log D, shake-flask Log D; KO, knock out; WT, wild type.

REFERENCES

- (1) Dementia statistics | Alzheimer's Disease International
<https://www.alz.co.uk/research/statistics> (accessed Aug 21, 2019).
- (2) Honig, L. S.; Mayeux, R. Natural history of Alzheimer's disease. *Aging: Clin. Exp. Res.* **2001**, *13*, 171–182.
- (3) Murray, P. S.; Kumar, S.; DeMichele-Sweet, M. A. A.; Sweet, R. A. Psychosis in Alzheimer's disease. *Biol. Psychiatry* **2014**, *75*, 542–552.

- (4) Lebois, E. P.; Thorn, C.; Edgerton, J. R.; Popiolek, M.; Xi, S. Muscarinic receptor subtype distribution in the central nervous system and relevance to aging and Alzheimer's disease. *Neuropharmacology* **2018**, *136*, 362–373.
- (5) Bodick, N. C.; Offen, W. W.; Levey, A. I.; Cutler, N. R.; Gauthier, S. G.; Satlin, A.; Shannon, H. E.; Tollefson, G. D.; Rasmussen, K.; Bymaster, F. P.; Hurley, D. J.; Potter, W. Z.; Paul, S. M. Effects of xanomeline, a selective muscarinic receptor agonist, on cognitive function and behavioral symptoms in Alzheimer disease. *Arch. Neurol. (Chicago)* **1997**, *54*, 465–473.
- (6) Shekhar, A.; Potter, W. Z.; Lightfoot, J.; Lienemann, J.; Dube, S.; Mallinckrodt, C.; Bymaster, F. P.; McKinzie, D. L.; Felder, C. C. Selective muscarinic receptor agonist xanomeline as a novel treatment approach for schizophrenia. *Am. J. Psychiatry* **2008**, *165*, 1033–1039.
- (7) Raedler, T. J.; Bymaster, F. P.; Tandon, R.; Copolov, D.; Dean, B. Towards a muscarinic hypothesis of schizophrenia. *Mol. Psychiatry* **2007**, *12*, 232–246.
- (8) Bridges, T. M.; LeBois, E. P.; Hopkins, C. R.; Wood, M. R.; Jones, J. K.; Conn, P. J.; Lindsley, C. W. Antipsychotic potential of muscarinic allosteric modulation. *Drug News Perspect.* **2010**, *23*, 229–240.
- (9) Conn, P. J.; Lindsley, C. W.; Meiler, J.; Niswender, C. M. Opportunities and challenges in the discovery of allosteric modulators of GPCRs for the treatment of CNS disorders. *Nat. Rev. Drug Discov.* **2014**, *13*, 692–708.
- (10) Menniti, F. S.; Lindsley, C. W.; Conn, P. J.; Pandit, J.; Zagouras, P.; Volkman, R. A. Allosteric modulation for the treatment of schizophrenia: targeting glutamatergic networks. *Curr. Top. Med. Chem.* **2013**, *13*, 26–54.

- (11) Mirza, N. R.; Peters, D.; Sparks, R. G. Xanomeline and the antipsychotic potential of muscarinic receptor subtype selective agonists. *CNS Drug Rev.* **2006**, *9*, 159–186.
- (12) Bender, A. M.; Jones, C. K.; Lindsley, C. W. Classics in chemical neuroscience: xanomeline. *ACS Chem. Neurosci.* **2017**, *8*, 435–443.
- (13) Sramek, J. J.; Hurley, D. J.; Wardle, T. S.; Satterwhite, J. H.; Hourani, J.; Dies, F.; Cutler, N. R. The safety and tolerance of xanomeline tartrate in patients with Alzheimer's disease. *J. Clin. Pharmacol.* **1995**, *35*, 800–806.
- (14) Bymaster, F. P.; McKinzie, D. L.; Felder, C. C.; Wess, J. Use of M1–M5 muscarinic receptor knockout mice as novel tools to delineate the physiological roles of the muscarinic cholinergic system. *Neurochem. Res.* **2003**, *28*, 437–442.
- (15) Levey, A. I. Muscarinic acetylcholine receptor expression in memory circuits: implications for treatment of Alzheimer disease. *Proc. Natl. Acad. Sci. U. S. A.* **1996**, *93*, 13541–13546.
- (16) Birdsall, N. J. M.; Bradley, S.; Brown, D. A.; Buckley, N. J.; Challiss, R. J.; Christopoulos, A.; Eglen, R. M.; Ehlert, F.; Felder, C. C.; Hammer, R.; Kilbinger, H. J.; Lambrecht, G.; Langmead, C.; Mitchelson, F.; Mutschler, E.; Nathanson, N. M.; Schwarz, R. D.; Tobin, A. B.; Valant, C.; Wess, J. Acetylcholine receptors (muscarinic) (version 2019.4) in the IUPHAR/BPS Guide to Pharmacology Database. *IUPHAR/BPS Guide to Pharmacology CITE*, *2019(4)*. Available from: <https://doi.org/10.2218/gtopdb/F2/2019.4>. (accessed Jan 29, 2020).
- (17) Wood, M. R.; Noetzel, M. J.; Melancon, B. J.; Poslusney, M. S.; Nance, K. D.; Hurtado, M. A.; Luscombe, V. B.; Weiner, R. L.; Rodriguez, A. L.; Lamsal, A.; Chang, S.; Bubser, M.; Blobaum, A. L.; Engers, D. W.; Niswender, C. M.; Jones, C. K.; Brandon, N. J.; Wood, M. W.; Duggan, M. E.; Conn, P. J.; Bridges, T. M.; Lindsley, C. W. Discovery of VU0467485

/AZ13713945: an M4 PAM evaluated as a preclinical candidate for the treatment of schizophrenia. *ACS Med. Chem. Lett.* **2016**, 8, 233–238.

(18) Tarr, J. C.; Wood, M. R.; Noetzel, M. J.; Bertron, J. L.; Weiner, R. L.; Rodriguez, A. L.; Lamsal, A.; Byers, F. W.; Chang, S.; Cho, H. P.; Jones, C. K.; Niswender, C. M.; Wood, M. W.; Brandon, N. J.; Duggan, M. E.; Conn, P. J.; Bridges, T. M.; Lindsley, C. W. Challenges in the development of an M4 PAM preclinical candidate: the discovery, SAR, and in vivo characterization of a series of 3-aminoazetidine-derived amides. *Bioorg. Med. Chem. Lett.* **2017**, 27, 2990–2995.

(19) Long, M. F.; Engers, J. L.; Chang, S.; Zhan, X.; Weiner, R. L.; Luscombe, V. B.; Rodriguez, A. L.; Cho, H. P.; Niswender, C. M.; Bridges, T. M.; Conn, P. J.; Engers, D. W.; Lindsley, C. W. Discovery of a novel 2,4-dimethylquinoline-6-carboxamide M4 positive allosteric modulator (PAM) chemotype via scaffold hopping. *Bioorg. Med. Chem. Lett.* **2017**, 27, 4999–5001.

(20) Melancon, B. J.; Wood, M. R.; Noetzel, M. J.; Nance, K. D.; Engelberg, E. M.; Han, C.; Lamsal, A.; Chang, S.; Cho, H. P.; Byers, F. W.; Bubser, M.; Jones, C. K.; Niswender, C. M.; Wood, M. W.; Engers, D. W.; Wu, D.; Brandon, N. J.; Duggan, M. E.; Conn, P. J.; Bridges, T. M.; Lindsley, C. W. Optimization of M4 positive allosteric modulators (PAMs): the discovery of VU0476406, a non-human primate in vivo tool compound for translational pharmacology. *Bioorg. Med. Chem. Lett.* **2017**, 27, 2296–2301.

(21) Salovich, J. M.; Vinson, P. N.; Sheffler, D. J.; Lamsal, A.; Utley, T. J.; Blobaum, A. L.; Bridges, T. M.; Le, U.; Jones, C. K.; Wood, M. R.; Daniels, J. S.; Conn, P. J.; Niswender, C. M.; Lindsley, C. W.; Hopkins, C. R. Discovery of *N*-(4-methoxy-7-methylbenzo[*d*]thiazol-2-

yl)isonicatinamide, ML293, as a novel, selective and brain penetrant positive allosteric modulator of the muscarinic 4 (M₄) receptor. *Bioorg. Med. Chem. Lett.* **2012**, *22*, 5084–5088.

(22) Wood, M. R.; Noetzel, M. J.; Poslusney, M. S.; Melancon, B. J.; Tarr, J. C.; Lamsal, A.; Chang, S.; Luscombe, V. B.; Weiner, R. L.; Cho, H. P.; Bubser, M.; Jones, C. K.; Niswender, C. M.; Wood, M. W.; Engers, D. W.; Brandon, N. J.; Duggan, M. E.; Conn, P. J.; Bridges, T. M.; Lindsley, C. W. Challenges in the development of an M₄ PAM in vivo tool compound: the discovery of VU0467154 and unexpected DMPK profiles of close analogs. *Bioorg. Med. Chem. Lett.* **2017**, *27*, 171–175.

(23) Bubser, M.; Bridges, T. M.; Dencker, D.; Gould, R. W.; Grannan, M.; Noetzel, M. J.; Lamsal, A.; Niswender, C. M.; Daniels, J. S.; Poslusney, M. S.; Melancon, B. J.; Tarr, J. C.; Byers, F. W.; Wess, J.; Duggan, M. E.; Dunlop, J.; Wood, M. W.; Brandon, N. J.; Wood, M. R.; Lindsley, C. W.; Conn, P. J.; Jones, C. K. Selective activation of M₄ muscarinic acetylcholine receptors reverses MK-801-induced behavioral impairments and enhances associative learning in rodents. *ACS Chem. Neurosci.* **2014**, *5*, 920–942.

(24) Birdsall, N. J. M.; Farries, T.; Gharagozloo, P.; Kobayashi, S.; Lazareno, S.; Sugimoto, M. Subtype-selective positive cooperative interactions between brucine analogs and acetylcholine at muscarinic receptors: functional studies. *Mol. Pharmacol.* **1999**, *55*, 778–786.

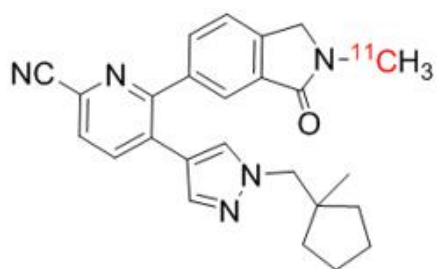
(25) Christopoulos, A.; Kenakin, T. G protein-coupled receptor allosterism and complexing. *Pharmacol. Rev.* **2002**, *54*, 323–374.

(26) Eckelman, W. C.; Gibson, R. E.; Rzeszotarski, W. J.; Vieras, F.; Mazaitis, J. K.; Francis, B.; Reba, W. C. The design of receptor binding radiotracers. In *Principles of Radiopharmacology*; Colombetti, L., Ed.; CRC Press: New York, 1979; Vol. 1, pp 251

- (27) Waterhouse, R. N. Determination of lipophilicity and its use as a predictor of blood-brain barrier penetration of molecular imaging agents. *Mol. Imaging Biol.* **2003**, *5*, 376–389.
- (28) Schubert, J. W.; Harrison, S. T.; Mulhearn, J.; Gomez, R.; Tynebor, R.; Jones, K.; Bunda, J.; Hanney, B.; Wai, J. M.-C.; Cox, C.; McCauley, J. A.; Sanders, J. M.; Magliaro, B.; O'Brien, J.; Pajkovic, N.; Agrapides, S. L. H.; Taylor, A.; Gotter, A.; Smith, S. M.; Uslander, J.; Browne, S.; Risso, S.; Egbertson, M. Discovery, optimization, and biological characterization of 2,3,6-trisubstituted pyridine-containing M4 positive allosteric modulators. *ChemMedChem* **2019**, *14*, 943–951.
- (29) Acton, J. J.; Bao, J.; Egbertson, M.; Gao, X.; Harrison, S. T.; Knowles, S. L.; Li, C.; Lo, M. M.-C.; Mazzola, R. D., Jr.; Meng, Z.; Rudd, M. T.; Selyutin, O.; Tellers, D. M.; Tong, L.; Wai, J. M.-C. 3-(1*H*-pyrazol-4-yl)pyridines as allosteric modulators of M4 muscarinic acetylcholine receptor and their preparation. WO2017107089 A1, 2017.
- (30) Zhang, L.; Villalobos, A.; Beck, E. M.; Bocan, T.; Chappie, T. A.; Chen, L.; Grimwood, S.; Heck, S. D.; Helal, C. J.; Hou, X.; Humphrey, J. M.; Lu, J.; Skaddan, M. B.; McCarthy, T. J.; Verhoest, P. R.; Wager, T. T.; Zasadny, K. Design and selection parameters to accelerate the discovery of novel central nervous system positron emission tomography (PET) ligands and their application in the development of a novel phosphodiesterase 2A PET ligand. *J. Med. Chem.* **2013**, *56*, 4568–4579.
- (31) Zhang, R.; Kavana, M. Quantitative analysis of receptor allosterism and its implication for drug discovery. *Expert Opin. Drug Discovery* **2015**, *10*, 763–780.
- (32) Pechter, D.; Xu, S.; Kurtz, M.; Williams, S.; Sonatore, L.; Villafania, A.; Agrawal, S. Applying dataflow architecture and visualization tools to in vitro pharmacology data automation. *J. Lab. Autom.* **2016**, *21*, 817–823.

(33) Hamill, T. G.; Sato, N.; Jitsuoka, M.; Tokita, S.; Sanabria, S.; Eng, W.; Ryan, C.; Krause, S.; Takenaga, N.; Patel, S.; Zeng, Z.; Williams, D., Jr.; Sur, C.; Hargreaves, R.; Burns, H. D. Inverse agonist histamine H3 receptor PET tracers labelled with carbon-11 or fluorine-18 *Synapse (Hoboken, NJ, U. S.)* **2009**, 63, 1122–1132.

Table of Contents graphic.



[¹¹C]13: [¹¹C]MK-6884
BP_{ND} = 0.83
(rhesus monkey)

